Thermal Analysis of Compacted Graphite Iron

by

Hamed Hoseini Hooshyar

Diploma work No. 60/2011
at Department of Materials and Manufacturing Technology
CHALMERS UNIVERSITY OF TECHNOLOGY
Gothenburg, Sweden

Diploma work in the Master program Advanced Engineering Materials

Performed at: Volvo Powertrain AB
405 08 Gothenburg

Supervisor(s): Dr Pål Schmidt
Volvo Powertrain AB
Dept. 91522, Z1.1, 405 08 Gothenburg

Examiner: Kenneth Hamberg
Assistant Professor
Department of Materials and Manufacturing Technology
Chalmers University of Technology, SE-412 96 Gothenburg

Thermal Analysis of Compacted Graphite Iron

Hamed Hoseini Hooshyar

Diploma work no 60/2011
Department of Materials and Manufacturing Technology
Chalmers University of Technology
SE-412 96 Gothenburg
Sweden
Telephone + 46 (0)31-772 1000

Cover:
[Microstructure of compacted graphite iron analysed by Optical Microscope.]

[Chalmers Reproservice]
Gothenburg, Sweden 2011

Thermal Analysis of Compacted Graphite Iron
Hamed Hoseini Hooshyar
Department of Materials and Manufacturing Technology
Chalmers University of Technology

Abstract

Because of several attractive properties, compacted graphite iron has found a significant role in different areas like automotive engines and machine parts. The main focus of this project is on characterizing Compacted Graphite Iron (CGI) samples by different thermal analysis techniques and also achieving some thermal analysis approaches. Casting trials were made in Skövde and special raw materials were used. The treatment was made by the sandwich method. Magnesium, inoculants and rare earth metals were added to the melt. Different samples were cast with different Mg levels and holding times to analyse the effect of these parameters on graphite formation and variation in nodularity. First some images were taken from the samples by optical microscope and scanning electron microscope to make the microstructure visible. Then image analysis was done by the Qwin software to observe the effect of those parameters. Finally, cooling curves related to the samples were analysed by Matlab software to be compared with each other. ATAS software also was used to extract the characteristic points of cooling curves to observe if it is possible to find a comparable correlation between different cast iron types. Finally it was concluded that flake graphite and spheroidal graphite irons are easily distinguishable from each other by means of comparing the characteristic points. Also some of those characteristic points are useful to distinguish between the flake graphite and compacted graphite irons but the recognition becomes difficult when the comparison is made between the compacted graphite and spheroidal graphite irons.

Keywords: Thermal Analysis, Compacted Graphite Iron

This thesis is dedicated
To
My parents

The Author gives his heartfelt appreciation to his parents who supported him with their love and encouraged him to pursue advanced degrees.

Acknowledgment

The author is grateful to Pål Schmidt, Ulla Boman and Kent Ericsson to let him participate in this project. Special thanks go to dear Pål Schmidt and Kenneth Hamberg for their continuous cooperation and technical and scientific support. The author also acknowledges all his colleagues at material department in Volvo Powertrain for providing him an intimate atmosphere during the project.

Abbreviations

CC……... Cooling Curve

CGI…….. Compacted Graphite Iron

FGI…….. Flake Graphite Iron

SGI……... Spheroidal Graphite Iron

TAL……..Temperature of Austenite Solidification

TEN or TES……Temperature of Eutectic Nucleation (Start)

TEU……. Temperature of Eutectic Undercooling

TER……. Temperature of Eutectic Arrest

TEE……..Temperature of Eutectic End

CG……Compacted Graphite

FG……Flake Graphite

SG……Spheroidal Graphite

Content:

I. Introduction

Compacted graphite iron (CGI) can be considered as a promising engineering material which contains graphite particles in compacted (vermicular) form. CGI shows intermediate mechanical and physical properties between grey and ductile irons. For instance, it possesses 70% higher tensile strength, 35% higher elastic modulus and nearly double fatigue strength of grey cast irons [1]. Thus it includes an optimal combination of different properties like strength, ductility and thermal conductivity which have lead to a distinctive attention during recent years. Because of these properties, CGI found a significant role in production of automotive engines, machine parts and also many different applications [2].

Nowadays, several methods of casting of CGI products have been developed, trying to find the best method to have a precise control on the final microstructure. In this project two methods based on thermal analysis will be discussed and the results related to the samples cast in the foundry will be analysed in order to find out whether the methods are applicable or not.

Thermal analysis is based on the principle that each phase transformation in a sample causes a thermal event on its cooling or heating curve. In fact, the cooling curve (CC) is a solidification history of its related sample. Thus it is feasible to obtain comparable information on cast iron by comparing the cooling curves of different graphite types. By means of the first and the second derivatives of the cooling curves, characteristic points correlated to cooling curves of different graphite types can be achieved and compared [3].

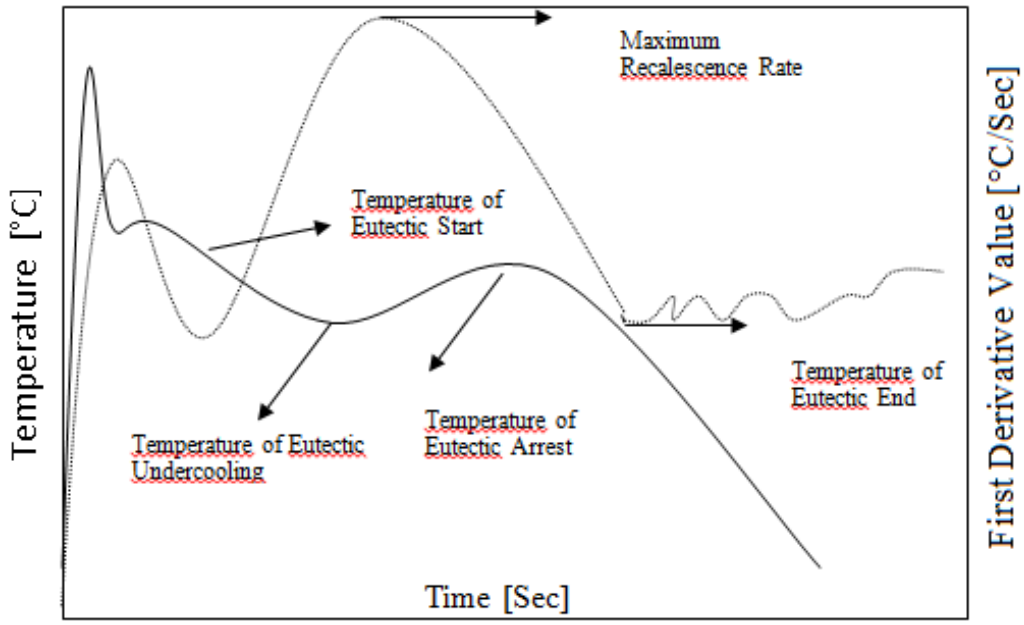

Figure 1. Typical cooling curve (continuous line) and its first derivative (dashed line) [3]

In figure 1, a typical CC of compacted graphite iron and its characteristic points are shown.

II. Literature Survey

2.1. Solidification Behavior of Hypoeutectic and Eutectic Compacted Graphite Cast Irons

An important tool to investigate the solidification process is thermal analysis in which the temperature during solidification is monitored. Any change in the solidification process causes an alteration in the slope of the curve. As can be seen from figure below, the solidification starts with formation of the primary austenite dendrites (TL or TAL). While decreasing the temperature, the dendrites grow and the melt is enriched with carbon. At TES, the graphite and austenite is formed. Finally at TEE point, the eutectic reaction ends.

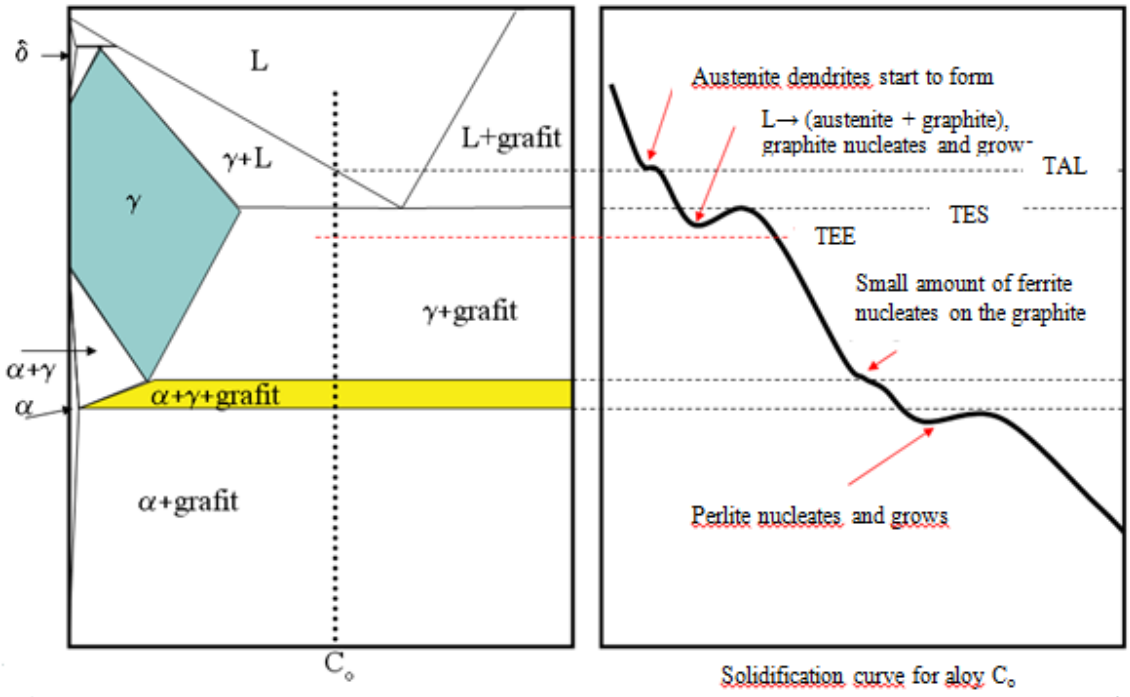

Figure 2 . Stable Fe-C system with addition of Si.

Regarding the intended cast iron type, some melt preparation is required. If the melt is treated with magnesium, vermicular and nodular cast iron will be formed. No addition of magnesium will lead to the grey iron. Another treatment step before solidification is inoculation. Here the number of nucleus for graphite is determined. At this work, the inoculant value has been kept constant, but different magnesium treatments were done which will be discussed in the future chapter.

2. 1. 1. Nucleation-Eutectic Cell Count

From figure 3, it can be seen that by decreasing the nodularity, the eutectic cell count is sharply decreased until it reaches the CG region. Then the drop becomes slower and finally it reaches the FG. Although there is a slight difference between eutectic count cell of FG and CG, the difference is very small in comparison with that of CG and SG. This shows that nucleation condition of CG is more like to FG than SG [4].

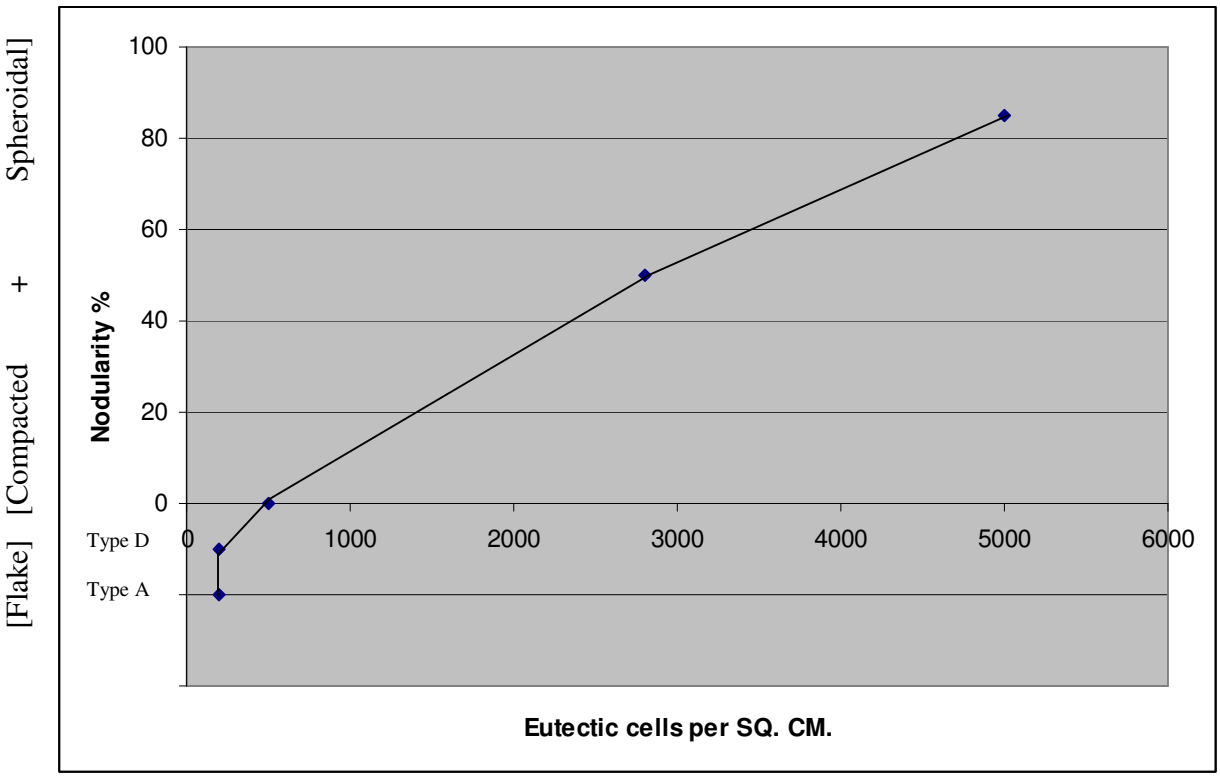

Figure 3. Correlation of eutectic cell count with different graphite structure in a CGI sample [4]

Now it can be easily understood why it is not feasible to decrease the chilling tendency of CGI by applying a strong post inoculation. That is because by increasing the amount of nuclei, the nucleation condition will be switched to typical condition for SG nucleation although the total chilling tendency will be decreased.

2. 1. 2. Growth of Graphite

The various possibilities of graphite growth in cast iron have been discussed by different researchers [5, 6].
The hexagonal graphite crystal probably grow by a screw dislocation mechanism along A or C axis [4]. The growth directions of hexagonal graphite has been shown in figure 4.

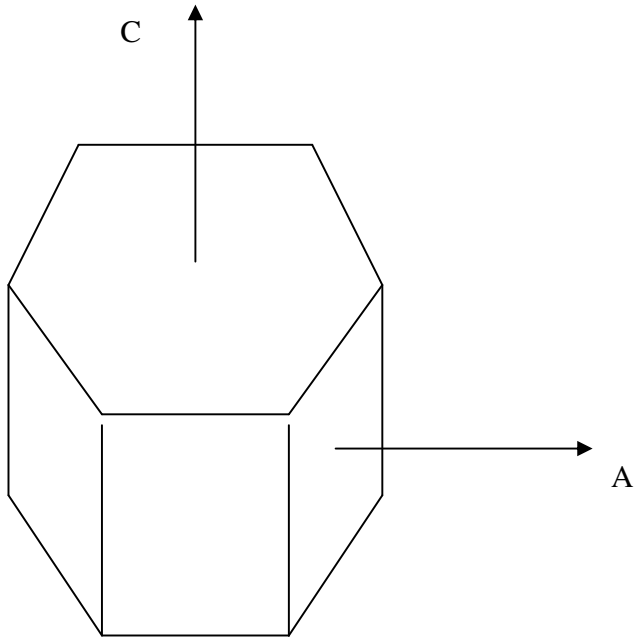

Figure 4. The growth directions of hexagonal graphite.

The eutectic cell growth in cast iron begins from a nucleus. In FGI, the graphite is in contact with the liquid during the solidification. The growth starts on a low number of nuclei, but because the growth condition in the liquid is fast it begins when the temperature go below the equilibrium temperature, with very low undercooling and recalescence. For FGI, the growth is mostly in 'A' direction [4].

For CGI, the growth condition is unfavourable. It means that it shows a delay in start of eutectic solidification compared to FGI. Because of that and low number of nuclei, a higher undercooling is required to proceed the solidification. Then the growth will proceed in preferential direction C axis (some authors believe that growth direction of CGI changes between A and C axis [7]). The graphite will grow in contact with the melt in the early stages of solidification. Then it grows rapidly and releases a lot of latent heat and resulting TER (Temperature of Eutectic Arrest) is considerably high [4].

The growth condition in SGI is also unfavourable, but because of a high number of nuclei (as was mentioned) the growth starts sooner and it does not need very low TEU (Temperature of Eutectic Undercooling) like CGI. Then it proceeds rather slowly with low TER since the graphite particles lose their contact with the liquid at the early stages of solidification [4].

In summary it can be stated that the nucleation condition of CGI is more like to that of FGI but the growth condition of CGI is more like to that o SGI.

Table 1 represents a summary of nucleation and growth conditions of different types of cast iron.

Table 1. Summary of solidification behaviour of hypoeutectic cast irons with various graphite shapes [3].

Type of Iron	Nucleation		Growth			Thermal Effects	
	No. Of Nuclei	No. Of Eutectic Cells	Conditions	Direction	Contact of Graphite with Liquid	Maximum Undercooling (TEU)	Recalescence
Flake Graphite	Low	Low	Favorable	A axis	Yes	Low	Intermediate
Compacted Graphite	Low	Low	Unfavorable	C axis	Yes	High	High
Spheroidal Graphite	High	High	Unfavorable	C axis	No	Low	Intermediate

2.2. CGI Structure

An acceptable CGI should contain less than 20% spheroidal graphite and more than 80% compacted graphite (without any flake graphite which can cause local weaknesses and lead to failure).Alloying elements have different effects on the structure ,for instance; copper, tin and molybdenum can act as matrix modifiers from ferritic to pearlitic [8-11].

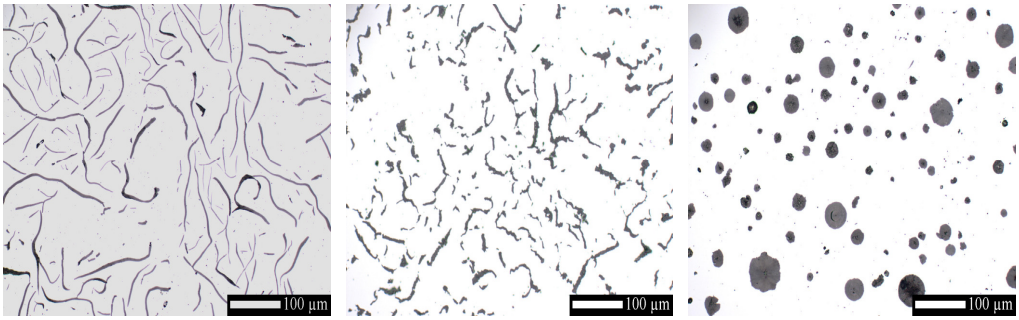

(I) **(II)** **(III)**

Figure 5. Typical graphite shapes;
I) Flake graphite type I ; II) Compacted graphite type III ; III) Spheroidal graphite type VI (graphite designation according to ISO standard)

Nodulizers include magnesium and rare earth metals such as cerium, lanthanum,etc.
Titanium can be added to the melt to inhibit the formation of nodules and cause formation of compacted graphite but on the other hand it should be noticed that it can lead to a ferritic matrix. Cu and Sn are pearlite stabilisers and added to the melt to change the matrix to a pearlitic one. Melt holding time, cooling rate, pouring time and pouring temperature are the other factors which can have a significant role on the formation of compacted graphite [1, 2, 8, 12-15].
One of the parameters which affect the morphology of the graphite in the structure is holding time of the melt. During the holding time, magnesium and inoculants fading may occur. It is found that it leads to some potential benefits like reducing the recalescence and also lower nodule count. On the other hand it should be noticed that high amount of

fading may change the nodules to flakes which is not favourable in CGI. It may also cause coarsening and micro-inclusion growth. Thus the right holding time should be selected for the melt before pouring [16].

2.3. CGI Stability

Figure 6 shows that the stable range of CGI is narrow. It should be considered that because of the fading effects, the initial starting point of the iron should be held far away from the flake region and in order to prevent forming a large number of nodules, the best position is CG+SG region. During holding, the microstructure will reach the CG plateau [17].Also it should be mentioned that the CGI plateau can be variable and different parameters like oxygen and sulphur content and amount of inoculants can shift it [18].

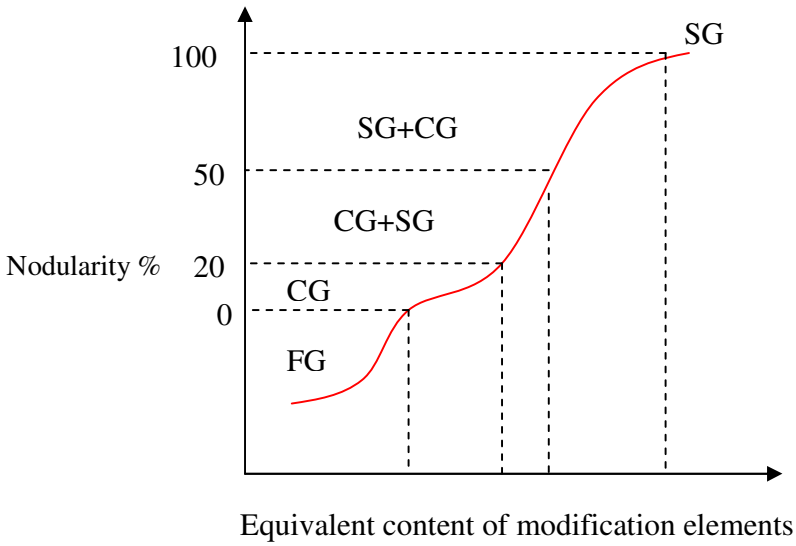

Figure 6, Modification level vs. equivalent content of modification elements [16]

2.4. Thermal Analysis-Approach I

Practically, one of the most effective methods for CGI production is closed loop controlling of modification level of graphite morphology in cast iron i.e. the first treatment should be done and instantly, as a first step, the melt quality must be evaluated. If it is found necessary, the modification level must be adjusted before pouring of the melt. After achieving the new melt characteristics, it can be finally poured into the mould [17].

Until now, a large number of studies have been done on evaluation of modification level in cast iron by thermal analysis technique [19]. For instance, Backerud[20], Kimura[21] and Stefanescu[22] have stated their own ideas about thermal analysis of cast iron, but

the point is that these findings can be achieved only under specific conditions and it is hard to observe the same result at different foundries.
Different parameters like charge materials, alloys used, melting process and treating method play significant roles on the shape of the thermal analysis cooling curves [23].
As was mentioned, it is difficult to find a correct correlation between cooling curves and melt quality (which includes indices like temperature, efficiency of inoculation and nodularization, temperature and the tendency of chill and shrinkage [17]) because different results can be achieved under different experimental conditions and in different foundries. A new method has been developed by X.J.Sun et al which simplify finding correlation between cooling curves and morphology of graphite in cast iron. It should be noticed that all factors affecting melt quality (as stated above), can have an influence on the shape of cooling curves. In his method, the freezing zone (a region in the cooling curve from liquidus to solidus temperature) is under focus and sampling temperature is considered as one of the melt quality parameters. Thus any variation in melt quality can lead to a distinctive change in cooling curve shape in the freezing zone and also it can be concluded that two melts which have similar cooling curve shapes have the same melt quality. Therefore, the unknown quality of the measured melt can be evaluated by information of known melt cooling curves (CCs). Parameter **Ω** can be defined to represent the amount of difference in the freezing zones of two cooling curves. If this amount is lower than the threshold, then it can be expected to have the same melt quality indices, including sampling temperature of the two melts [24].

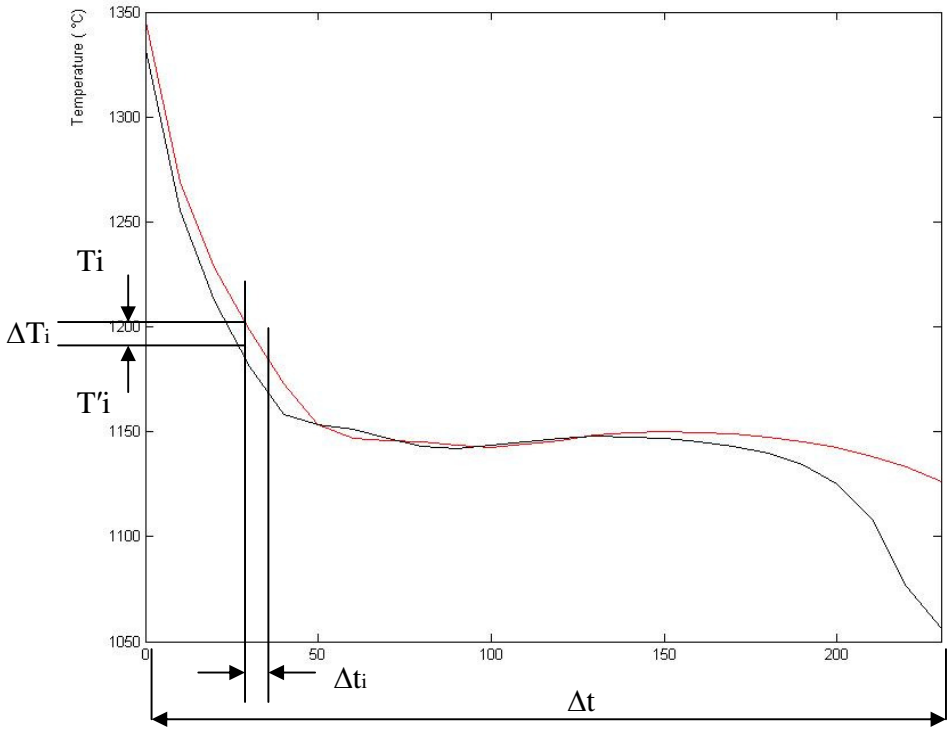

Figure 7. A schematic diagram of the cooling curve pattern recognition method

(Shape term) $$S= [[\sum (\Delta Ti - \Delta T)^2] / (n-1)]^{1/2} \quad (1)$$

(Temperature difference at pint i) $$\Delta Ti=Ti-T'i \quad (2)$$

(Mean temperature difference) $$\Delta T= (\sum \Delta Ti)/ n \quad (3)$$

$$\Omega=| [\sum \Delta Ti)/ n]| +S \quad (4)$$

(Parameter n refers to the number of compared points.)
Parameter Ω consists of two parts; the first part represents the average vertical distance and the second part shows the difference in shapes of two cooling curves.
For instance figure 8 shows the two cooling curves related to two different melts. The value of parameter Ω is very low (0.3 ºC) and thus these two cooling curves are significantly similar. Also the liquidus temperature for both of them is about 1141 ºC.

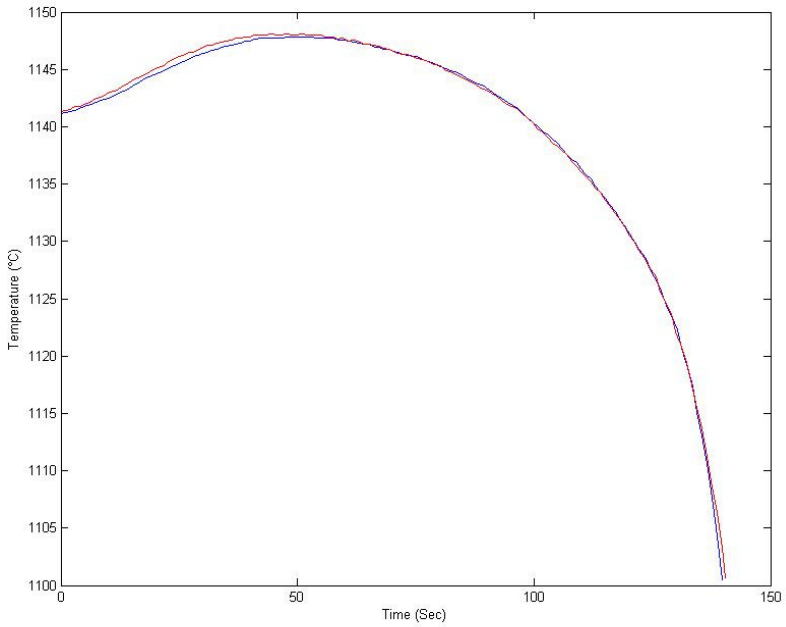

Figure 8.Two heats with similar thermal analysis cooling curves, Ω=0.3 ºC

As a first step, a database of records related to the freezing zone of intended melts and also the melt quality parameters set up. Then a thermal analysis sample is poured and the thermal analysis cooling curve is achieved. Finally, the freezing zone is evaluated and compared with references data to extract suitable melt quality indices. It is observed that without going into details about characteristic parameters of a cooling curve and its derivatives, melt quality indices of an unknown melt can be acquired. In other words, it can be said that this approach is just based on the comparison of the shapes of freezing zones. Thus, in contrast to previous methods, it can be applicable under different experimental conditions and foundries [26].

2.5. Thermal Analysis-Approach II

As mentioned above, thermal analysis of cooling curves is carried out as a means to control the melt quality and prevent unwanted structure and defects. Characteristic temperatures related to CCs have been stated by different authors [27, 28,29].
Table 2 and 3 describes some of these designations and figure 9 represents these points on a cooling curve and its first and second derivatives

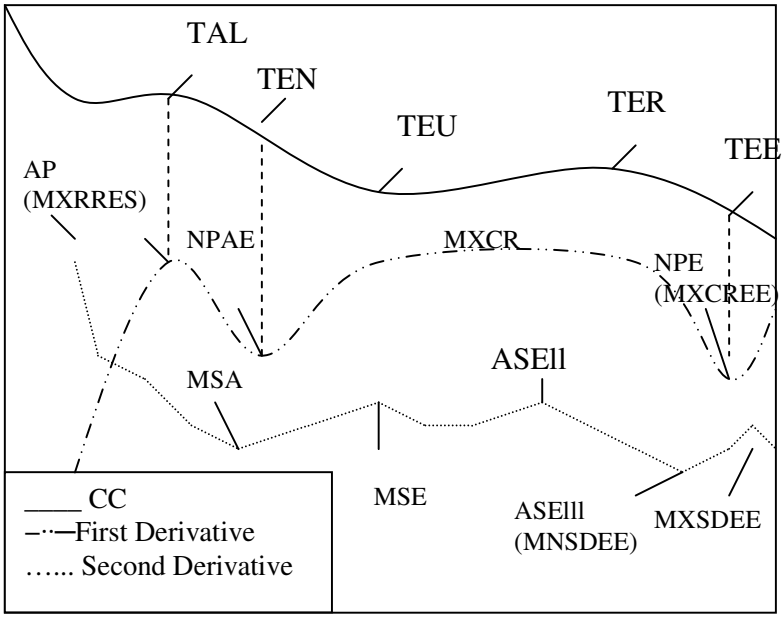

Figure 9. Typical hypoeutectic ductile iron cooling curve and its derivatives [30] The abbreviations are explained in tables 2 and 3.

Table 2.CC typical temperature points [30]

Name or acronym	Physical signification
Tmax	Maximum measured temperature
TAL	Temperature of primary austenite solidification in hypoeutectic and eutectic irons
TGL	Temperature of primary graphite solidification in hypoeutectic irons
TEN (TES)	Temperature of eutectic nucleation
TEU	Temperature of eutectic undercooling
TE	Eutectic Temperature
TER	Maximum temperature of eutectic arrest
TEE (TES)	Temperature of the end of eutectic solidification
TEN-TEU	Eutectic undercooling
TER-TEU	Eutectic recalescence

Table 3. Typical points of CC first and second derivatives [30]

Name or acronym	Physical signification
First derivative	
AP (MXRRES)	Austenite peak; area under this peak is reperesentative of the heat generated during solidification of autenite
NPAE	Negative peak between austenite to eutectic solidification, solidification changes from austenite to eutectic
MXCR	Maximum rate of recalescence
NPE (MXCREE)	Negative peak after eutectic. End of eutectic solidification corresponds to TEE
Second derivative	
MSA	Maximum slope of austenite peak
MSE	Maximum slope of eutectic peak
ASEII	Average slope of eutectic peak in stage II
MXSDEE	Maximum of second derivative at the end of eutectic solidification
ASEIII	Average slope of eutectic peak in stage III

In this approach the characteristic points of cooling curves are compared with each other to find a correlation between these points and different cast iron types.
The parameters which have influence on the shape of cooling curves include;
Mg treatment, Chemical composition of the iron, inoculation treatment, oxidation state of the melt, sulphur level, temperature of the melt, sampling method and cup geometry and cooling rate of the sample. Thus it is clear that there are many factors which affect CCs and their effects can even overlap. Therefore it is difficult to have a precise control of the quality by evaluation of characteristic points and process parameters [30]. Nevertheless, many commercial methods, like SinterCast, use this approach.

2. 5. 1. INTERPRETAION OF COOLING CURVES

As mentioned, compacted graphite cast iron has been considered as an intermediate form between spheroidal and flake graphite cast irons. It was observed that the properties related to CGI are located between those two types. Bäckerud, Nilsson and Steen [31] found that the cooling curves of CGI are also placed between FGI and SGI, but it is only right when applying a technique in which the crucible with a centrally placed thermocouple is immersed in a molten metal, but not when a cold mold is used [4].
More works on compacted graphite cooling curves demonstrated that the CGI's cooling curves do not usually lie between those for flake and spheroidal graphite.
Comparing the cooling curves, it can be seen that at the same chemical analysis and pouring temperature, the temperature of eutectic arrest (TER) and temperature of end of eutectic (TEE) for CGI is placed between those of SG and FG irons. But the temperature of eutectic undercooling (TEU) is the lowest one which is because of unfavourable nucleation condition in CG iron (it will be discussed later in this dissertation). It seems

safe to state that solidification of CGI has a delay in comparison of the other two types but when it starts to solidify ,it proceeds rapidly with a lot of latent heat released which results in higher TER than SGI [4].

Cooling curves of cast irons were used by Stefanescu to show the stable and metastable solidification. It was illustrated that if TES, TEU, TER and TEE are above the metastable temperature, the solidification and the final structure is gray, but if these characteristic points are below the metastable line, the iron structure will end as white iron. [3] The stable and metastable temperatures are based on chemical composition and can be found in reference: [32].

As mentioned above, the TER in CG iron is intermediate between SG and FG irons but TEU is lower than that for the other two types. It has been observed in some cases that the TER of CG iron is even lower than that of SG iron.

CG iron also has the lowest TES in comparison with SG and FG irons and it can be because of the delay in start of eutectic solidification of CG iron [3].

Also the TEE of CGI is close to that of FGI and both of them are significantly higher than that of SG iron. The low TEE of spheroidal graphite iron can indicate its tendency to formation of intercellular carbides [3].

The first derivatives of cooling curves can be divided in to two parts for a useful interpretation. The first part is a domain in which the temperature change increase until it reaches the maximum recalescence rate and the second one is the part in which the temperature change decreases. In CG iron, there is one slope in the second part of first derivative while SG, FG and even white irons have two slopes [3].

Another important parameter for comparison of different graphite types is maximum recalescence rate. It is considerably higher for CG iron, lower for FG iron and much lower for SG iron and white iron[3].

The latent heat can also be measured by multiplying the area under the first derivative with the specific heat of cast iron. It means that the area is proportional to the value of heat released during recalescence. Stefanescue showed that CG iron has the highest value among the other types and followed by FG iron. SG and white iron have the lowest value of latent heat [3].

It can be interesting to state here that there is also a significant difference between the gray(stable) and white(metastable) solidification, where as by increasing the cooling rate the characteristic points, which are, temperature of eutectic inoculation(TES),temperature of eutectic undercooling(TEU),temperature of eutectic recalescence(TER) and temperature of end of eutectic (TEE), will be decreased [4].

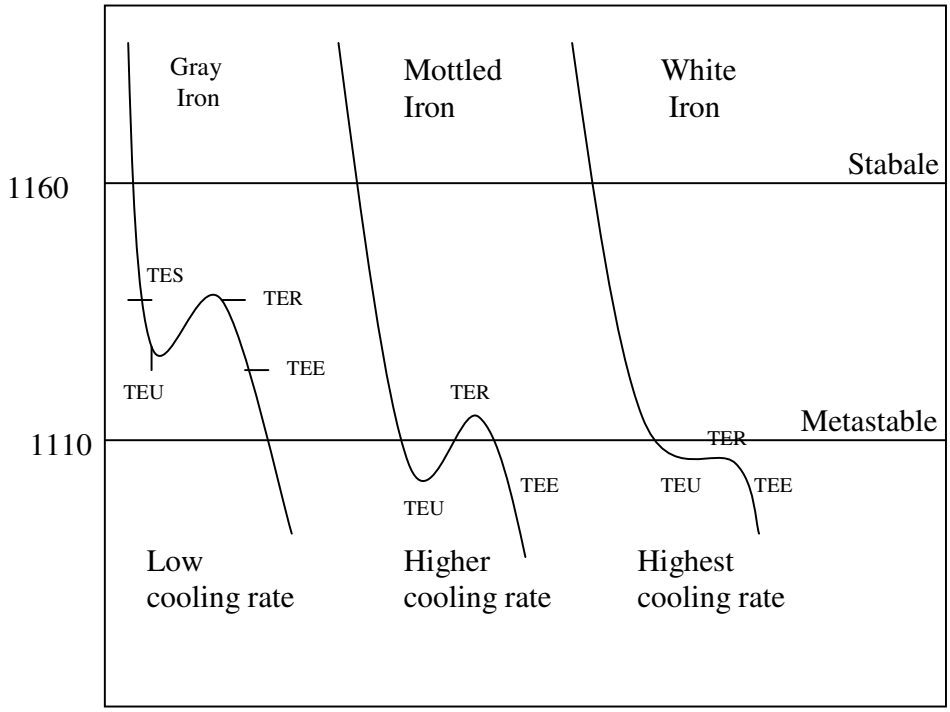

Figure 10. Effect of cooling rate on characteristic points and microstructure of cast iron [4]

2. 5. 2. Chilling tendency

There is a controversy here for CGI because by increasing the amount of Mg the chilling tendency must be increased but it is obvious that in CGI the chilling tendency is higher in comparison with ductile iron. It can be described by unfavourable noculation condition for CGI. (It was discussed in solidification section) [4].
Stefanescu et all showed that by increasing the nodularity the chilling tendency will be decreased, then reached a maximum for CGI and sharply decreased when the final product is FGI. Some post inoculation process can partially shadow the chilling effect [4].

III. Experimental procedure

The casting trials were made in Skövde on 2009-2010-2011. Special CGI raw material was melted in induction furnace MF2. Treatment was made with the sandwich method in a 1 ton ladle. Magnesium was added in the form of FeSiMg. In the treatment pocket was also added inoculant and rare earth metals. The pocket was then covered by steel sheets.
Different treatments were made, aiming at different Mg levels. After each treatment three ATAS cups were poured and an oxygen measurement was made. For each treatment, this cycle was repeated two times, giving three ATAS samples separated in time by approximately six to eight minutes. By this procedure the effect of fading was also taken into account.
The ATAS cup is 64.7 mm high and 51.5 mm wide with wall thickness of about 7 mm. An ATAS mould can be seen in picture below.

Figure 11. ATAS Cup

Therefore different samples were cast with different Mg levels and holding time to analyse the effect of these parameters on graphite formation and variation in nodularity. In one of the treatments, one ATAS cup was quenched in water after reaching the temperature of eutectic end to be compared with the cup cooled in a normal way to observe the effect of secondary graphite growth. The correlated amounts have been listed in table 3.
After cutting, mounting and polishing, samples were investigated by optical microscope. Three images for each sample were taken from different parts of the sample and it was tried to choose areas which represent the whole sample. Then, image analyses were done on the samples by Leica QWin Software to define the amount of nodularity. (Magnification=100, frames=9*9)

To make the microstructure visible, ATAS 1 was etched by Nital 3% for 10 seconds and analysed by Optical Microscope (OM) and a random sample was etched by a solution containing HCl and HNO_3 (Aqua regia) for 45 minutes to be analysed by Scanning Electron Microscope (SEM).
For the first approach, all ATAS cooling curves were drawn in the Matlab software and compared by each other to demonstrate the correlation of the nodularity difference and the parameter Ω (discussed in literature survey section).
For the second approach, ATAS software was used to extract the charactresitic points of all cooling curves to observe if it is possible to distinguish any correlation between different graphite types in samples cast at the foundry.

IV. Results and discussion

Figure 12 shows the microstructure of one analysed sample. Carbon in cast irons can be in the form of graphite or cementite. The laminated pearlitic matrix, a little amount of ferrite, nodular and compacted graphites are obvious in these pictures. In pictures A and B, a layer of ferrite covering the graphite nodules can be seen. This implies that carbon solved in matrix which are located around nodular graphite, can easily diffuse to those nodules and form a layer of ferrite around them. These structures are known as bull's-eye structures. Spherodising process can be considered because of the removal of sulphur and oxygen from the melt. Addition of Mg as a nodulizer can cause it and have the same effect.

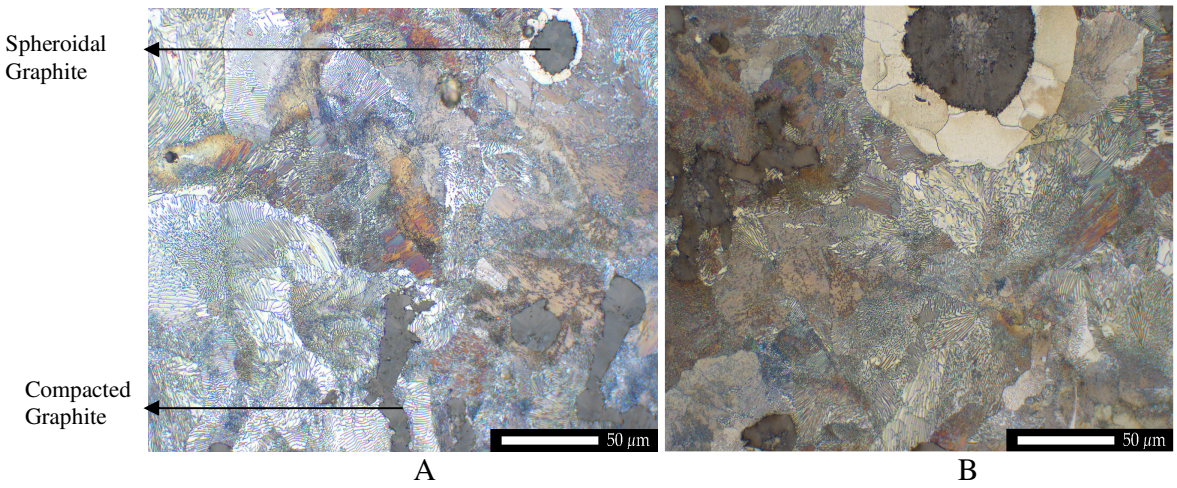

Figure 12. Microstructure of hypoeutectic CGI analysed by Optical Microscope.(Sample ATAS 1)

Compacted graphites, as it is shown in figure 12, have a shape between nodular and flake graphite and hence they are also known as quasi-flake graphite.
It should be noted that for production of compacted graphite iron, the amount of nodularity has a certain limit (20 %) and other elements like titanium is used to minimise the formation of nodules.
In figure 13, compacted graphites can be clearly seen. The first plot has been selected on vermicular shape and the chart related shows that the maximum peak belongs to carbon. The second plot which is selected on the matrix has Fe as a major element (pearlitic matrix).

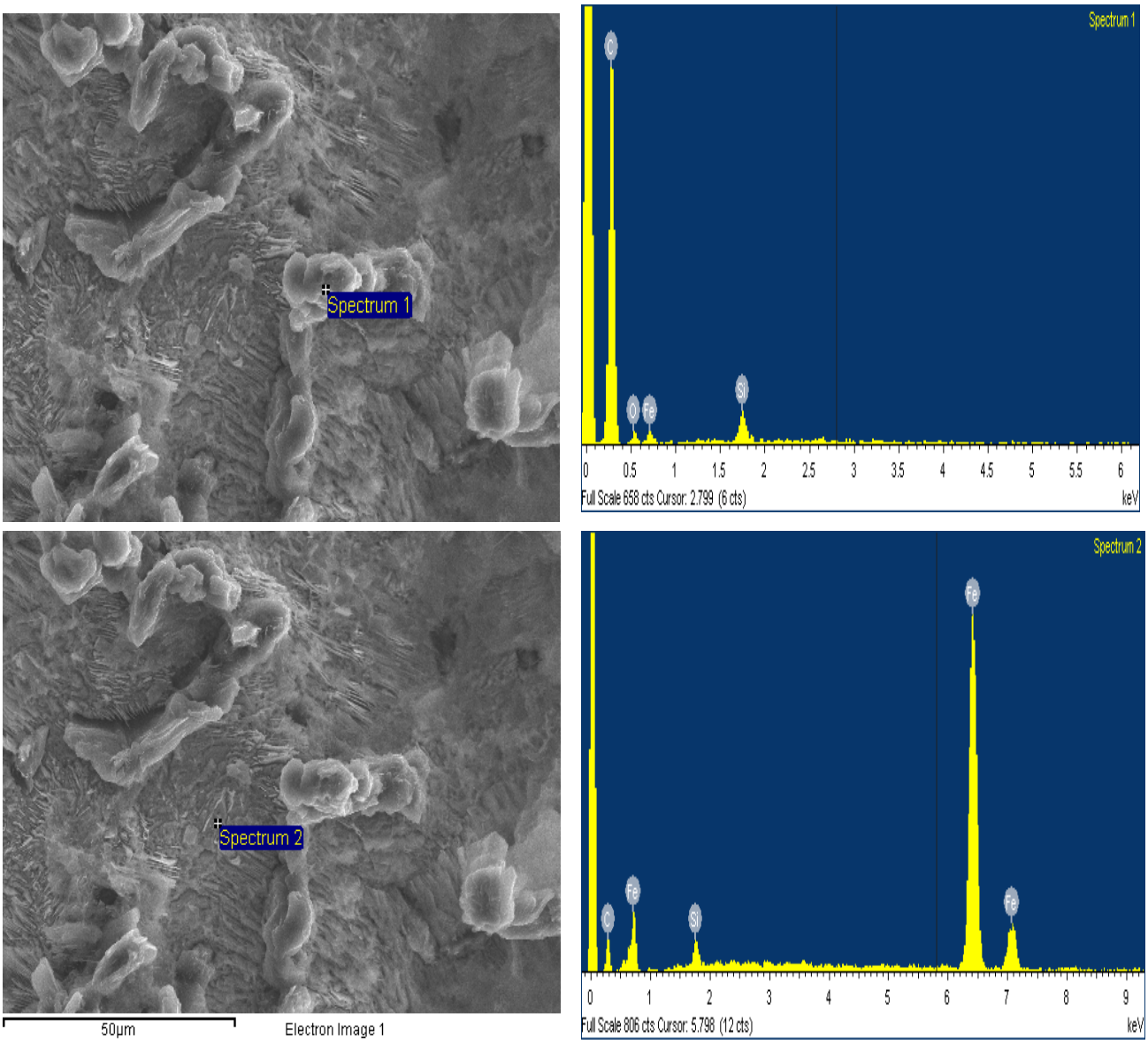

Figure 13 .Analysis of compacted graphite iron by SEM.

Figures 14 represent the graphite morphology transition due to different amount of Mg and holding time. The higher amount of magnesium, the more amount of nodularity will be achieved. It has been tried to have only Mg variation as a major parameter. The chemical composition and nodularity value of the samples can be found in table 4 and 5 respectively.

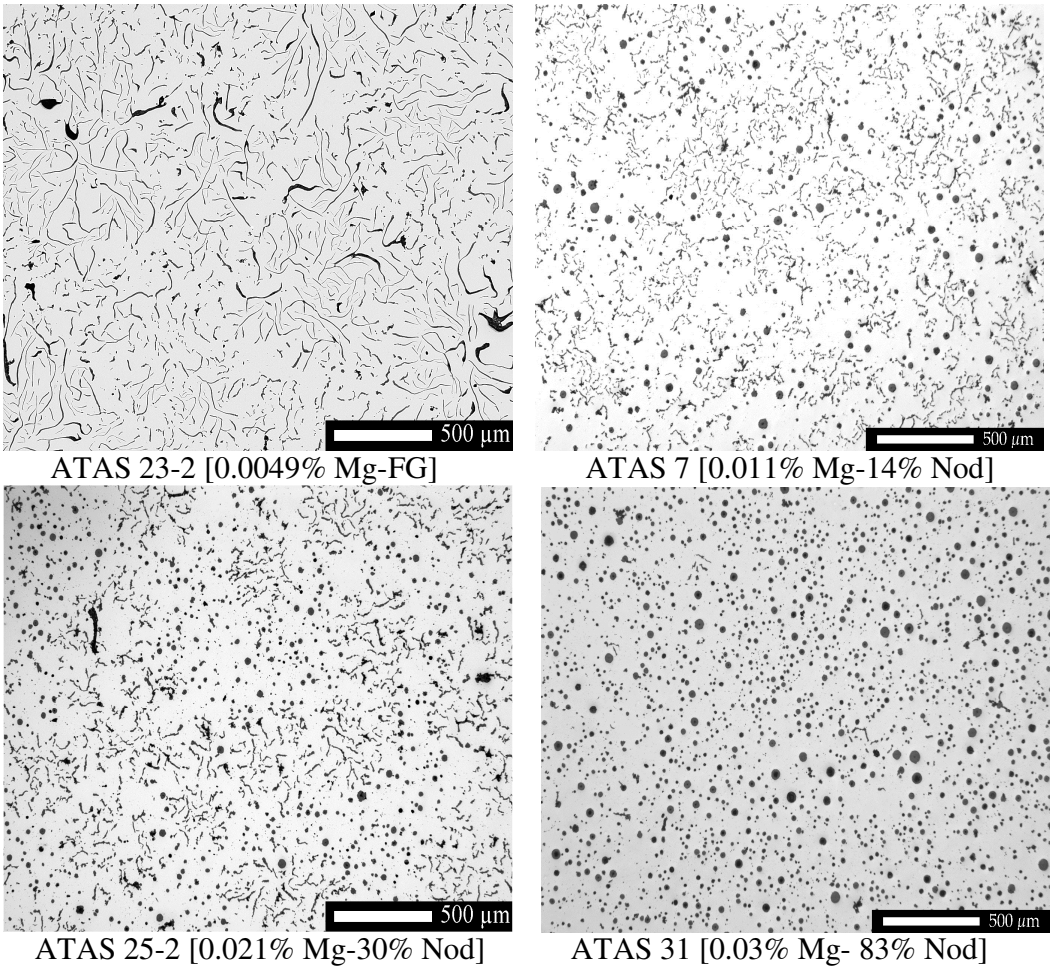

Figure 14 . Graphite morphology in different ATAS samples.

It should be pointed out that in this project; it was intended to do the magnesium treatment with different magnesium levels to have all three different cast iron types.

As it can be seen in figure 14, by increasing the magnesium content, the microstructure varies from flake to vermicular to spheroidal graphite. For example, ATAS 23-2, which was treated with low amount of magnesium (0.0049 % Mg), contains graphite in flake shape (grey iron). ATAS 7, which was treated with higher magnesium value (0.011 %Mg), contains graphite in vermicular and spheroidal shape and its nodularity value is 14% (the term ´´nodularity´´ will be discussed in the next chapter). As discussed, this microstructure can be considered as compacted graphite iron. Finally, ATAS 31 that contains the highest amount of magnesium (0.03 %Mg), has graphite in spheroidal shape and is called ductile iron. Some other images related to the other samples have been presented in appendix 1.

In table 4, the chemical composition of different ATAS samples is shown. It is well-known that carbon and silicon are the main alloying elements in cast iron. As mentioned, it was aimed to have just magnesium variation and keep the other parameters constant.

Table 4. Chemical composition of ATAS samples.

ATAS No.	C	Si	Mn	P	S	Cr	Ni	Mo	Cu	Sn	Ti	Mg	C_{ekv}
1	3,67	2,20	0,38	0,005	0,009	0,03	0,02	0,01	0,96	0,059	0,02	0,009	4,22
2	3,80	2,28	0,36	0,006	0,010	0,03	0,02	0,01	0,91	0,056	0,022	0,010	4,37
3	3,61	2,22	0,36	0,005	0,008	0,03	0,02	0,01	0,92	0,061	0,022	0,009	4,17
4	3,72	2,22	0,40	0,005	0,011	0,03	0,02	0,01	0,96	0,059	0,02	0,010	4,27
5	3,59	2,25	0,35	0,005	0,011	0,03	0,02	0,01	0,94	0,062	0,02	0,009	4,15
6	3,62	2,23	0,38	0,006	0,010	0,04	0,02	0,01	0,94	0,059	0,02	0,009	4,18
7	3,69	2,23	0,37	0,006	0,009	0,03	0,02	0,01	0,96	0,061	0,02	0,012	4,25
8	3,65	2,26	0,38	0,006	0,010	0,04	0,02	0,01	0,93	0,060	0,023	0,012	4,21
9	3,68	2,26	0,38	0,006	0,010	0,04	0,02	0,01	0,93	0,060	0,022	0,012	4,21
11	3,71	2,02	0,38	0,007	0,011	0,04	0,02	0,01	0,89	0,047	0,014	0,009*	4,21
12	3,70	2,02	0,41	0,008	0,011	0,04	0,02	0,01	0,88	0,048	0,015	0,009*	4,21
13	3,64	2,04	0,42	0,007	0,011	0,04	0,02	0,01	0,87	0,048	0,015	0,008	4,15
14	3,67	1,98	0,38	0,007	0,009	0,04	0,02	0,01	0,88	0,048	0,014	0,007	4,16
15	3,69	2,05	0,41	0,008	0,010	0,04	0,02	0,01	0,88	0,048	0,015	0,010	4,20
16	3,67	2,04	0,40	0,008	0,010	0,04	0,02	0,01	0,88	0,048	0,015	0,009	4,15
21	3,74	2,10	0,36	0,005	0,008	0,03	0,03	0,01	0,87	0,043	0,009	0,012	4,26
22	3,66	2,08	0,36	0,005	0,008	0,03	0,03	0,01	0,87	0,041	0,009	0,010	4,18
23	3,76	1,93	0,33	0,005	0,009	0,03	0,03	0,01	0,86	0,036	0,008	0,004	4,24
24	3,70	1,97	0,36	0,005	0,009	0,03	0,03	0,01	0,87	0,041	0,009	0,004	4,19
25	3,73	2,10	0,36	0,02	0,010	0,05	0,02	0,01	0,82	0,041	0,010	0,015	4,25
26	3,75	2,13	0,36	0,005	0,010	0,03	0,03	0,01	0,86	0,040	0,009	0,014	4,28
31	3,78	2,24	0,42	0,005	0,011	0,03	0,03	0,01	0,87	0,050	0,010	0,021	4,31
33	3,72	2,02	0,39	0,005	0,011	0,03	0,03	0,01	0,88	0,051	0,008	0,005	4,22
34	3,69	2,03	0,38	0,005	0,011	0,03	0,03	0,01	0,88	0,049	0,008	0,005	4,20
35	3,76	2,04	0,38	0,005	0,010	0,03	0,03	0,01	0,89	0,051	0,008	0,008	4,27

It should be mentioned that;

- The carbon equivalent values are roughly close to each other in all samples.
- The magnesium content of the samples written in table above refers to the residual magnesium after casting and these values were measured by means of XRD technique.
- The magnesium content range, which plays the most important role in this study, varies between 0.004 to 0.021%.

4.1. Image analysis

Volvo Material Technology is today using an Image analysis system from Leica (Leica Qwin 2.8). Because of the heterogeneity of the cast samples, there are always a scattering in the nodularity value in different parts of the samples. For example, it becomes critical when the nodularity of an engine block is checked in the production line, since it can be scrapped even when it has just a few nodularity percentages higher than the standard demand. Nevertheless it may meet the requirement if the scattering in nodularity is considered.
Scattering in nodularity in each sample can be because of different parameters like the casting method (inoculation, Mg treatment, ladle design), the segregation of magnesium around the perimeter of the austenite unit cell etc. which all leads to a heterogeneous structure. It is obvious from the images below that a large number of graphite nodules encompass the compacted ones and as mentioned it is due to the magnesium segregation phenomena.

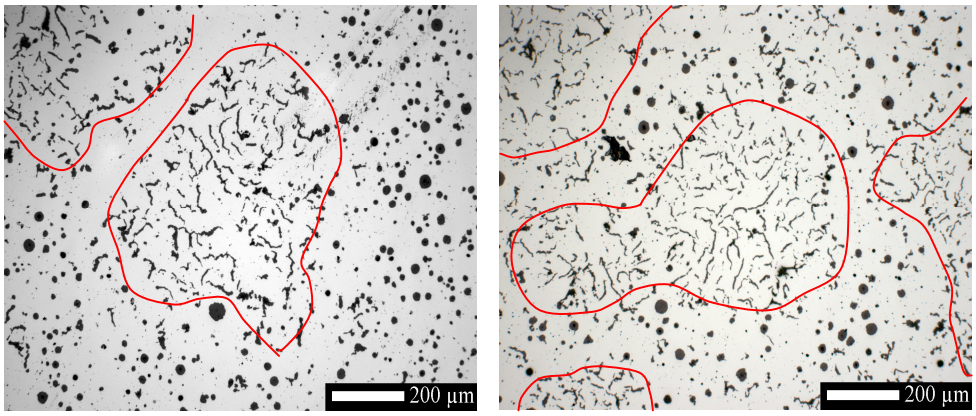

Figure 15. Segregation of magnesium.

ISO standard recommends using the roundness factor as the basis for the measurement of nodularity. The equation below represents the definition of roundess [35].

$$\text{Roundness} = (4 \times A)/(\pi \times L_m^2)$$

A = Area of the graphite feature; L_m = Max feret of the graphite feature

The ISO16112:2006 standard specifies intervals for the Roundness. Intervals used in the ISO-nodularity are:

Roundness	Graphite roundness shape factor	Form
0 - 0,525	III (I and II not included)	Compacted
0,525 - 0,625	IV and V	Intermediate
0,625 - 1	VI	Nodular

Now the percentages of nodularity can be defined;

Nodularity %= $((\Sigma A_{nodular} + 0{,}5 \times \Sigma A_{intermed})/(\Sigma A_{all})) \times 100$

For the Volvo-nodularity the follwing roundness classes are used:

Roundness	Form
0 - 0,575	Compacted (Flake graphite not allowed)
0,575 - 1	Nodular

Nodularity %= ((Number of features with Roundness > 0,575)/ (Total number of features)) x 100.

Thus as can be seen from the equations, the area of features is used in the ISO-nodularity instead of the count of features in the Volvo-nodularity. Volvo method used to be applied for nodularity measurement but nowadays ISO standard method is used.
Here are some arguments for using ISO-standard instead of Volvo method for nodularity measurement:

- It seems logical that the amount (and shape) of the graphite, rather than the number of particles, should be related to properties like tensile strength and thermal conductivity. If the number of particles is counted, very small particles (dirt) will have a big influence.
- It is an ISO standard which means it is widely accepted. For instance, Sintercast Company uses this method.

For a quantitative analysis of the amount of scattering, 10 different samples were analysed based on the Volvo and ISO methods. For each sample, image analysis was done four times starting from four different corners and each time 36 images were taken to be sure that the analysis had covered the whole sample (the total number of images for each sample is 144 images). The results can be seen in figure 16 and 17.

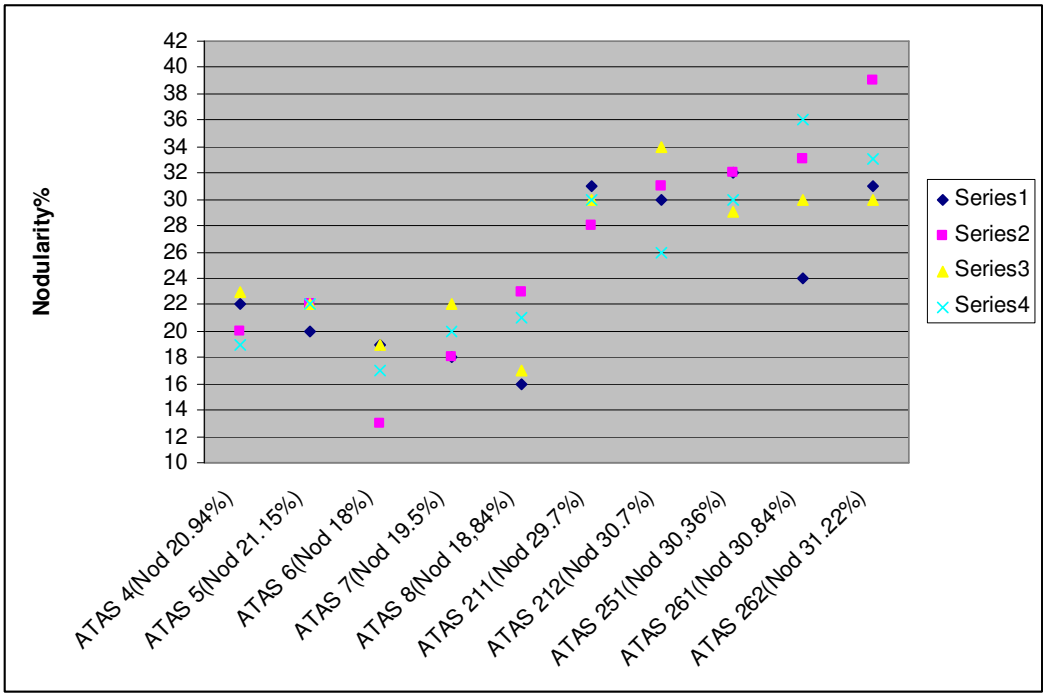

Figure 16. Nodularity of 10 different samples, starting from four different corners (based on Volvo method)

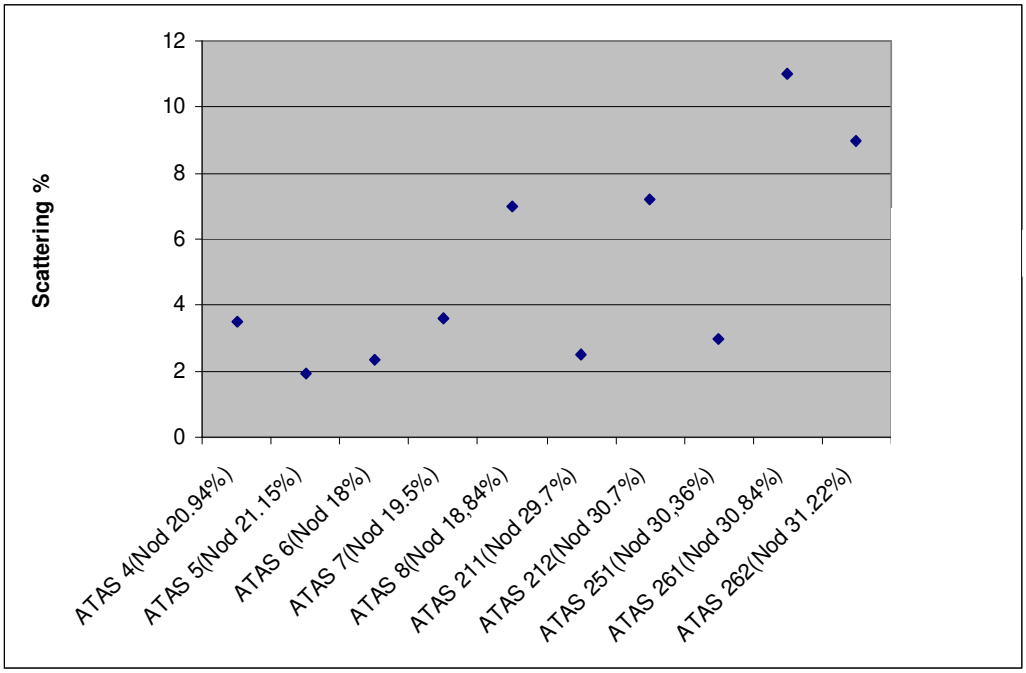

Figure 17. The amount of scattering in 10 different samples (based on Volvo method).

The scattering showed in figure 17 is expressed as the difference between maximum and minimum nodularity of each sample. As can be seen, the value in some samples like number 262, 261, 212 and 8 is considerable.
The same experiment was done one more time using the ISO standard method. Chart 18 shows that the amount of scattering in nodularity is significantly higher when the analysis is done based on the ISO standard method.

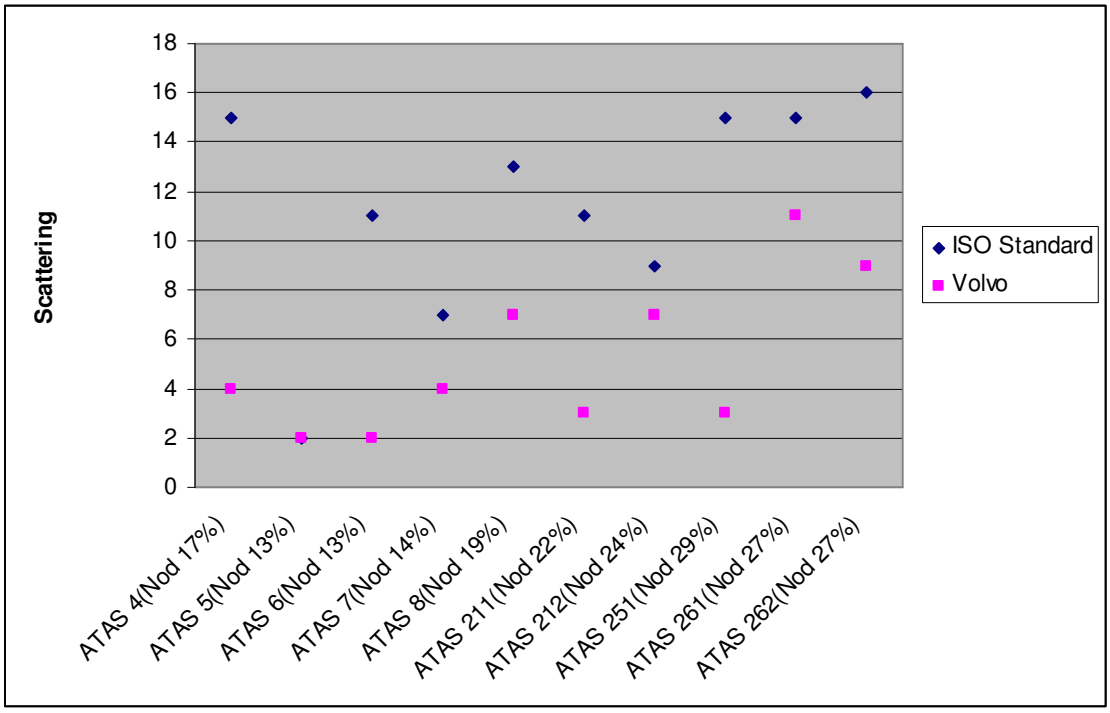

Figure 18. Comparison of scattering in nodularity using two different image analysis methods.

It can be concluded that proper selection of the image analysis technique can play an important role to decrease scattering and achieve a reliable nodularity value.
Increasing the number of image fields can also be a solution for achieving a stable nodularity value. But how many images are adequate for reaching the goal? The answer can be extracted in the graphs below.

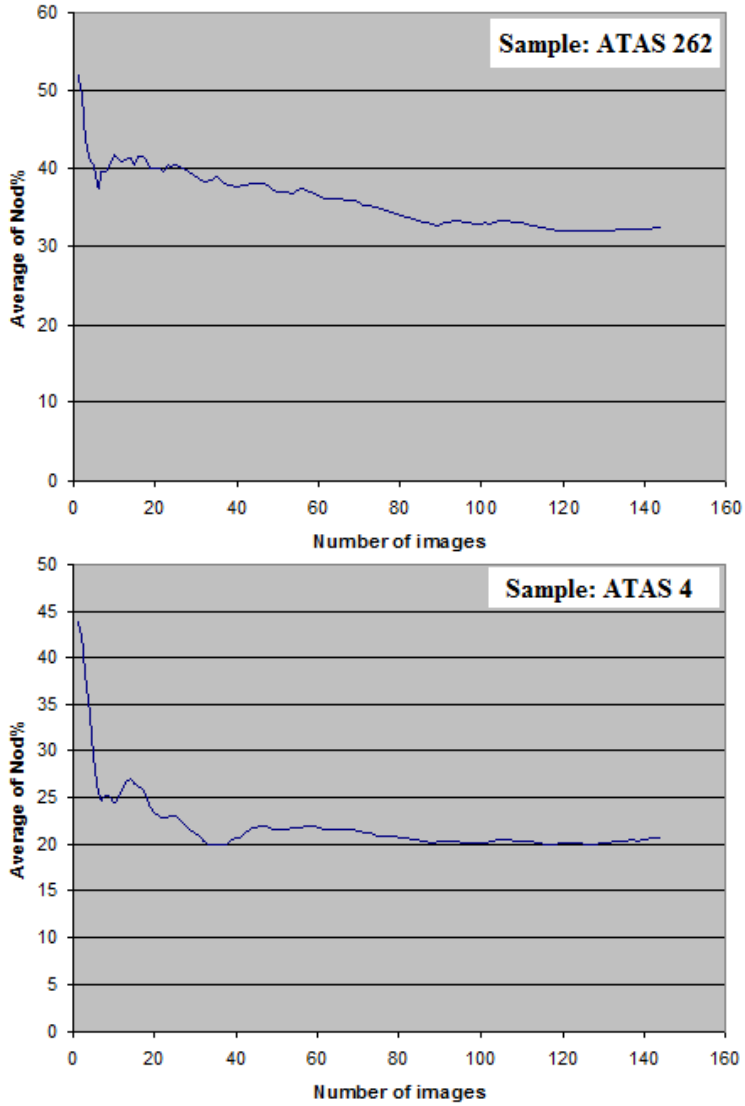

Figure 19. The average of nodularity versus the number of images for sample ATAS 262 and ATAS 4 based on the Volvo method.

It is obvious that the more number of images, the more accurate results will be achieved. The total number of images taken from each sample in this analysis is 144. It can be seen that after a specific number of images, the average of nodularity will become nearly constant. Depending on the accuracy needed, the number of images can be selected.
The chart below shows that there is the same behaviour also when the ISO standard is used for nodularity measurement.

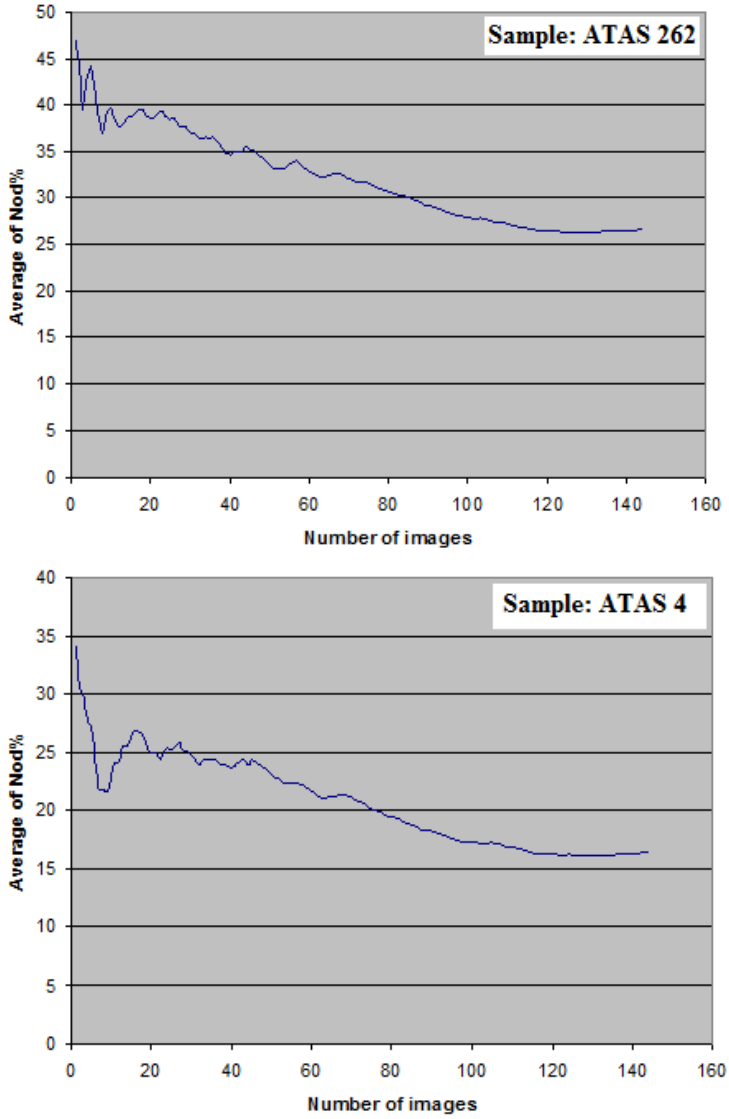

Figure 20. The average of nodularity versus the number of images for sample ATAS 262 and ATAS 4 based on the ISO standard method.

More charts have been presented in appendix 2.

It should be considered that even in one specific sample the shape of the curve depends on which side of the sample the analysis starts. In chart 21, which is related to sample ATAS 6, it can be seen four different curves starting from four different corners of the sample.

If it is supposed that the accepted nodularity percentage of the sample is between 10% to 20% and the total number of images used in analysis is just 25, then none of the blue and the green curves is in the acceptable range, although if the right number of images is selected, they will be in the range.

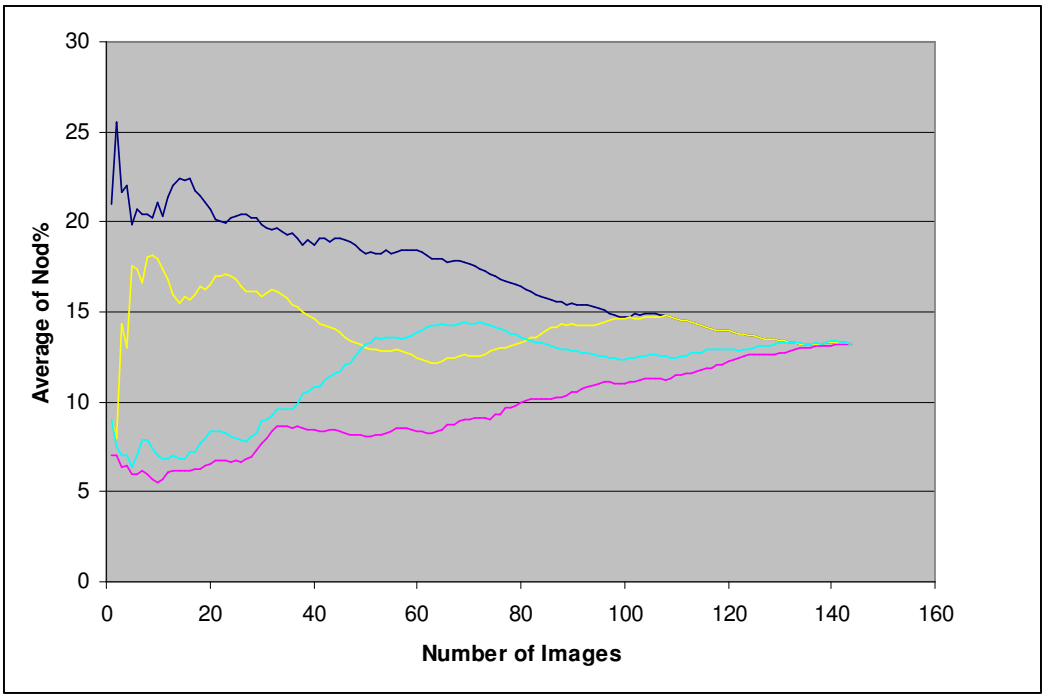

Figure 21. The average of nodularity versus the number of images for sample ATAS 6 based on the ISO standard method. Each curve represents a different starting point.

It can be concluded that there are always some scattering in nodularity value of the samples because of the heterogeneity of their microstructure. The scattering seems to be higher when the ISO standard method is used.

One way to achieve a stable nodularity value is increasing the number of image fields. It can be seen that just in one sample (ATAS 5, see appendix 2), the 'real' value of nodularity can be achieved below 40 images (based on ISO standard method) and for the rest of them more than 120 images are needed. Although increasing the number of images for analysis can be a reliable way to achieve the real value of the nodualrity, it makes the experiments unordinary time-consuming.

On the other hand, e.g. in a production situation, it is necessary to measure a reliable nodularity value. Therefore a solution to compensate for the scattering must be found.

In this project 81 numbers of images were used for determination of nodularity value. Although it was time consuming, it worthed because it is tried to observe the effect of different parameters on the nodularity value of the samples, then it is logical to decrease the effect of scattering as much as possible. (It should be mentioned that in previous works done by the author, 25 numbers of images were taken and evaluated but the results did not show any reasonable trend. Thus in this study the number of images was increased and as can be seen in figure 16, the results came close to the results written in literatures and became more applicable for this project.)

Table 5 shows the nodularity value of all ATAS samples based on ISO standard method. The magnesium level represent the total magnesium added in the ladle (FeMgSi(Kg)/Melt (kg)).

Table 5. Definition of ATAS Samples.

ATAS No.	*Mg%*	*Holding Time[min]*	*Treatment*	*Nodularity %*
1	*0.0094*	*0*	*N*	*14*
2	*0.0094*	*6*	*N*	*14*
3	*0.0094*	*12*	*N*	*13*
4	*0.0099*	*0*	*N*	*17*
5	*0.0099*	*6*	*N*	*13*
6	*0.0099*	*12*	*N*	*13*
7	*0.011*	*0*	*N*	*14*
8	*0.011*	*6*	*N*	*14*
9	*0.011*	*12*	*N*	*13*
11	*0.0065*	*0*	*N*	*11*
12	*0.0065*	*6*	*N*	*11*
13	*0.0083*	*0*	*N*	*8*
14	*0.0083*	*6*	*N*	*12*
15	*0.0114*	*0*	*N*	*9*
16	*0.0114*	*6*	*N*	*11*

***Q: Quenched**
***N: Normal**

ATAS No.	*Mg%*	*Holding Time[min]*	*Treatment*	*Nodularity %*
211	***0.019***	***0***	***Q***	***22***
212	***0.019***	***0***	***N***	***24***
221	***0.019***	***8***	***Q***	***18***
222	***0.019***	***8***	***N***	***20***
231	***0.0049***	***0***	***Q***	***FG(plus some CG and SG)***
232	***0.0049***	***0***	***N***	***FG(plus some CG and SG)***
241	***0.0049***	***8***	***Q***	***FG***
242	***0.0049***	***8***	***N***	***FG***
251	***0.021***	***0***	***Q***	***29***
252	***0.021***	***0***	***N***	***30***
261	***0.021***	***8***	***Q***	***27***
262	***0.021***	***8***	***N***	***27***

****Q: Quenched***
****N: Normal***

ATAS No.	*Mg%*	*Holding Time[min]*	*Treatment*	*Nodularity %*
311	***0.03***	***0***	***N***	***83***
312	***0.03***	***0***	***N***	***82***
313	***0.03***	***0***	***N***	***81***
321	***0.03***	***6***	***N***	***68***
322	***0.03***	***6***	***N***	***63***
323	***0.03***	***6***	***N***	***64***
331	***0.0059***	***0***	***N***	***FG***
332	***0.0059***	***0***	***N***	***FG***
333	***0.0059***	***0***	***N***	***FG***
341	***0.0059***	***6***	***N***	***FG***
342	***0.0059***	***6***	***N***	***FG***
343	***0.0059***	***6***	***N***	***FG***
351	***0.011***	***0***	***N***	***11***
352	***0.011***	***0***	***N***	***12***
353	***0.011***	***0***	***N***	***12***
361	***0.011***	***6***	***N***	***11***
362	***0.011***	***6***	***N***	***13***
363	***0.011***	***6***	***N***	***11***

****Q: Quenched***
****N: Normal***

4. 2. Effect of Magnesium Addition and Holding Time on Nodularity value.

As expected, by increasing the magnesium content in the samples the nodularity value is increased. The trend in the ATAS samples can be seen in figure 16.

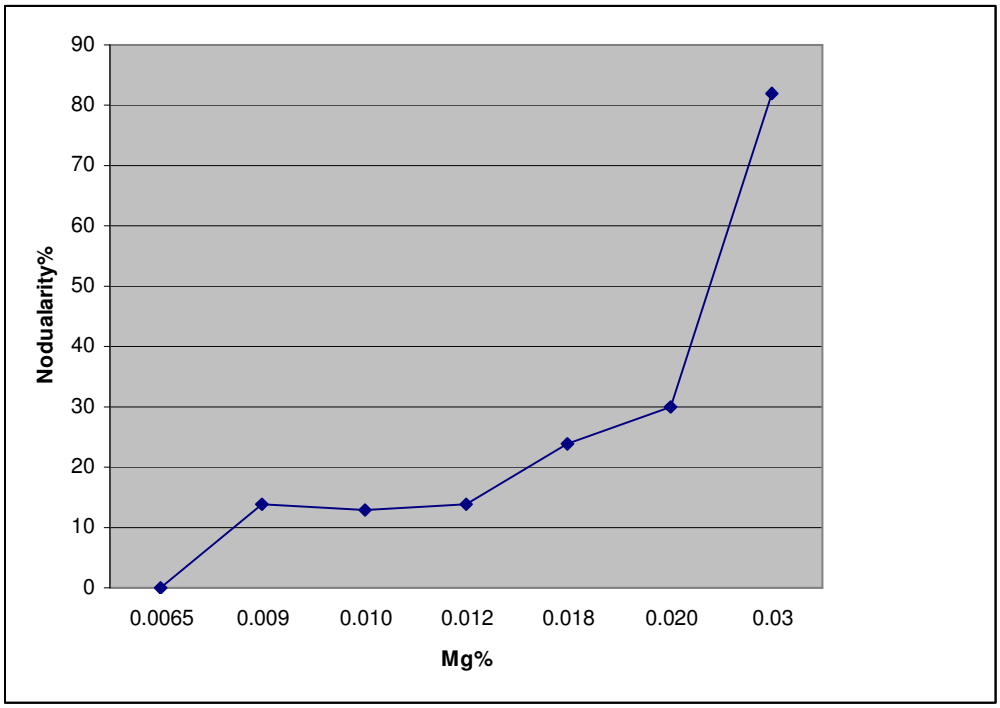

Figure 22. The correlation between Magnesium (added) % and Nodularity % in ATAS samples.

As can be seen in figure 22, the CGI window is quite larger than it was expected and if it is supposed that it is accepted to have CGI sample with up to 30 % nodularity, then the Mg accepted range is between 0.009 % to 0.020 %. Thus it is possible to target the middle of this range to have just one step casting process (without correction method).
The effect of fading due to holding time is not obvious in samples contain low amount of magnesium but it is considerable in samples with high Mg content.
The fading rate in the first minutes is fast but after a period of time, it reaches a plateau. It can be because of high burning speed of nodulisers and inoculants and also stable modification level over a range of those elements [33].
In figure 23, each pair of bars have the same Mg content. The white one shows nodularity directly after vermicularizing treatment and the black one shows nodularity after holding for about 6 minutes (the definition of ATAS samples can be seen in table 4). It can be observed, in the samples 312 and 322 which contain high Mg content, the fading is considerable and a drop of about 20 % in nodularity has been occurred. But in samples with lower Mg %, there is not any significant change in nodularity value.

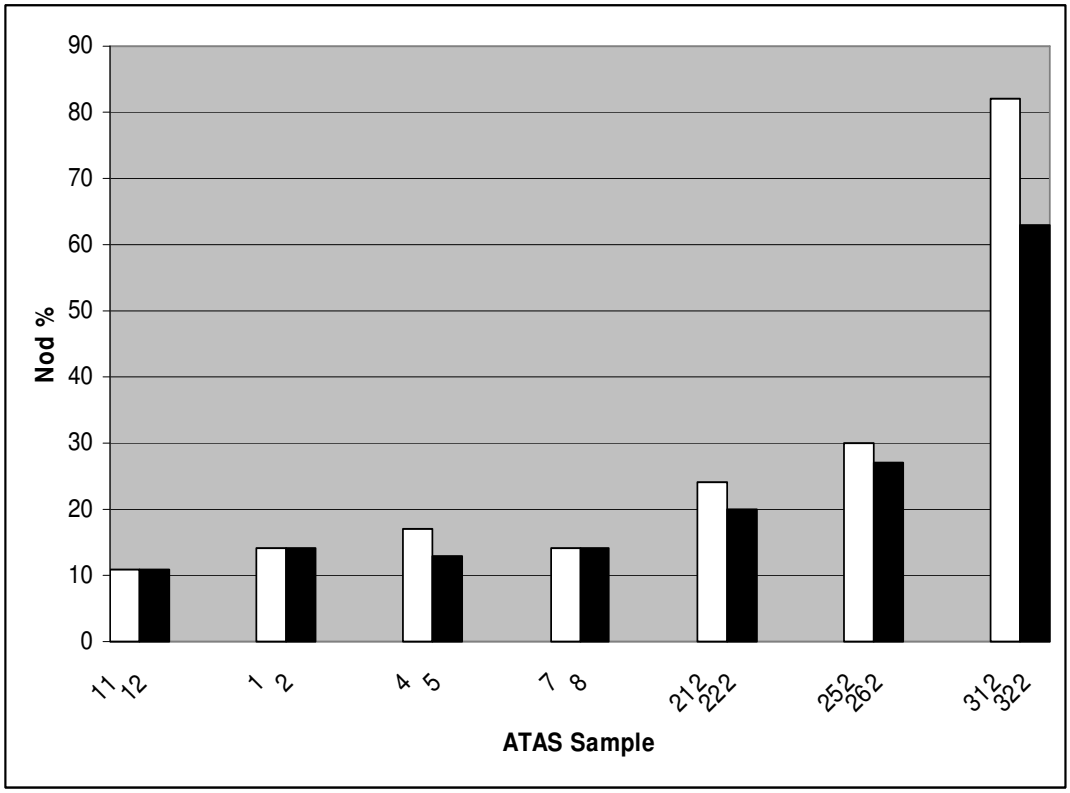

Figure 23. Fading Effect, the white column demonstrate nodularity right after vermicularizing treatment and the black one refers to the nodularity after holding for about 6 min (with the same Mg content).

4. 3. Primary and Secondary Graphite Growth

Within the eutectic reaction, the eutectic austenite integrates the primary austenite and form the matrix. In this step, dispersed graphite particles also form in the austenitic matrix. Within the eutectoid reaction, the austenite which contains about 0.68% carbon, change into the ferrite and graphite (secondary graphite).

The cooling curves discussed in the project, contain the first zone i.e the area between the melt liquidus temperature and the temperature of eutectic end. It has been intended to check whether the secondary graphite has any significant effect at the final microstructure or not.

To proceed, in one of the casting series, one of the ATAS samples of each trial was quenched in water right after reaching the TEE point. The treatment prevents the formation of secondary graphite at the final microstructure. The difference in graphite area between quenched and non-quenched samples and also the nodularity values can be seen in the graphs 24 and 25.

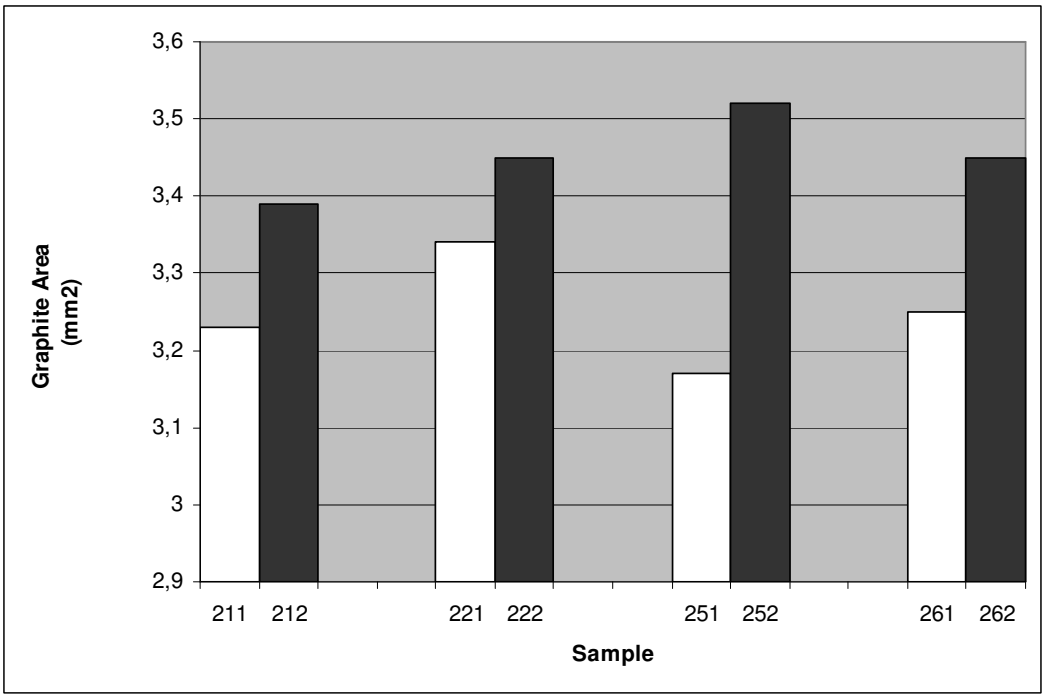

Figure 24. Change in graphite area for samples quenched in water (white column) and samples cooled at foundry atmosphere (black column). (Total measured area= 37.17 mm2)

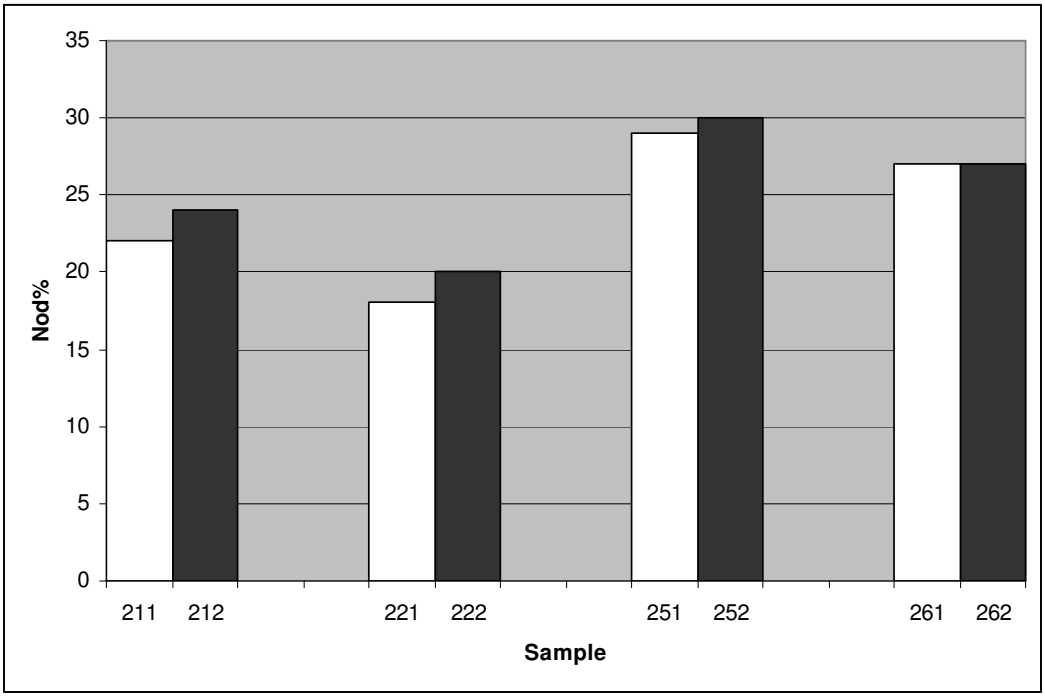

Figure 25 . Change in nodualrity value for samples quenched in water (white column) and samples cooled at foundry atmosphere (black column)

It is clear that there is a slight increase in graphite area for the non-quenched samples. But the difference is negligible and does not have any significant effect on the final

microstructure. It is accepted in the literatures that the most of the secondary graphites are integrated into the primary one and cause thicker particles at the end of the solidification process. Also the variation in nodularity is also minor and it can be considered just as a scattering issue discussed in image analysis section.
Then it can be concluded that the eutectic reaction play the most important role for the final graphite microstructure and it is logical to just consider the freezing zone (starting from TAL to TEE) rather than the whole cooling curve.

4. 4. Thermal Analysis-Approach I

Approach I has been precisely evaluated and is at the moment confidential. Any questions can be answered by Pål Schmidt.

4. 5. Thermal Analysis-Approach II

As mentioned in the literature survey, some authors has stated that since the properties of the CGI is intermediate between SGI and FGI, the cooling curve related to a CGI sample also locates between those of the other two types [31]. Other authors believe that this happens just under a specific condition of casting [4].
It is clear from figure 26 that CCs of CGI samples cast in the project fall between the CCs of FGI and SGI. The CCs have nearly the same starting point temperature.

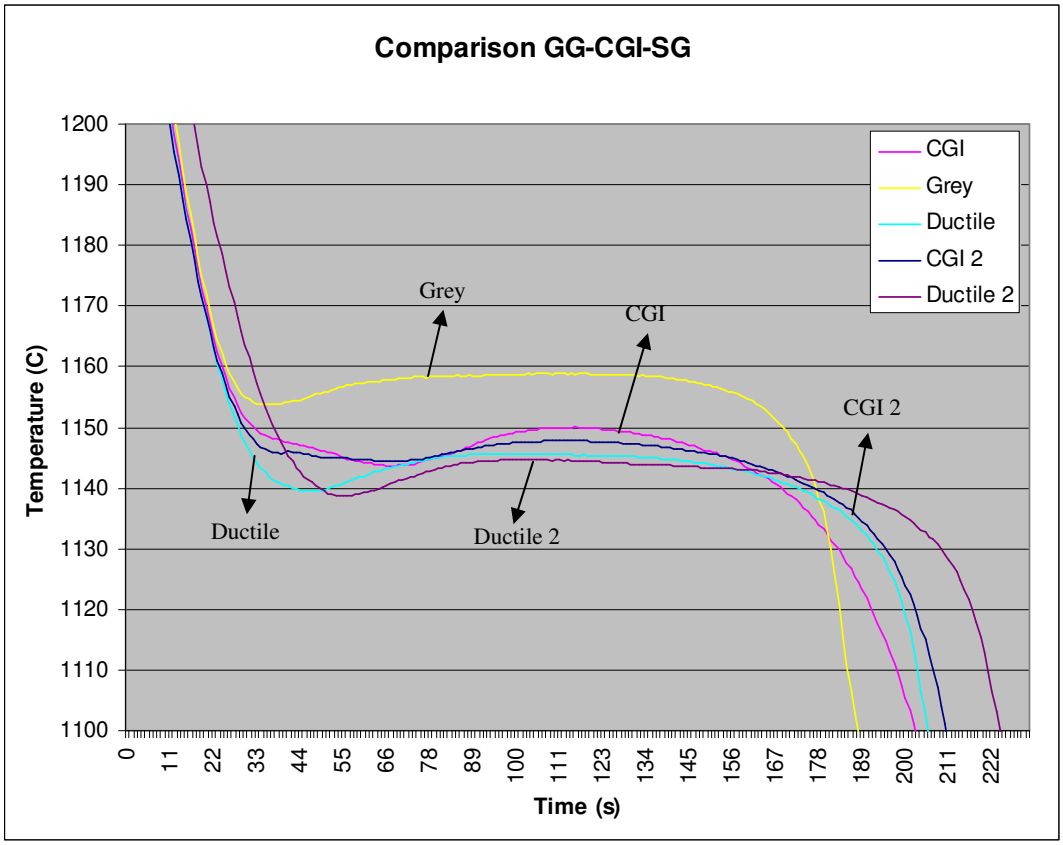

Figure 26. CCs of different cast iron types with nearly the same starting point temperature.

However, it should be considered that the shape of the cooling curve is dependent not only on the Mg treatment, but also on parameters like chemical composition of the iron, inoculation treatment, oxidation state of the melt, sulphur level, temperature of the melt, filling ratio, sampling method and cup geometry. In samples cast in the project, it was tried to have variation just in Mg and inoculant value and keep the other parameters constant. However, sampling temperature, filling ratio and carbon equivalent were some parameters that were difficult to keep constant.
The main purpose in this approach is to compare the characteristic points on the CCs to find a logical correlation between the points and the nodularity value and to see if it is possible to distinguish the different cast iron types by evaluation of the characteristic temperatures. Some of the characteristic points are discussed below.

4. 5. 1. Temperature of Primary Austenite Solidification (TAL or TL)

By increasing the CE value, the temperature of austenite solidification decreases, but Mg as a noduliser element does not play a direct role on variation of the TAL. Although in most cases the TAL of CGI locates below the one of FGI, there are many overlaps which make the comparison impossible. The value slightly decreases for SGI.

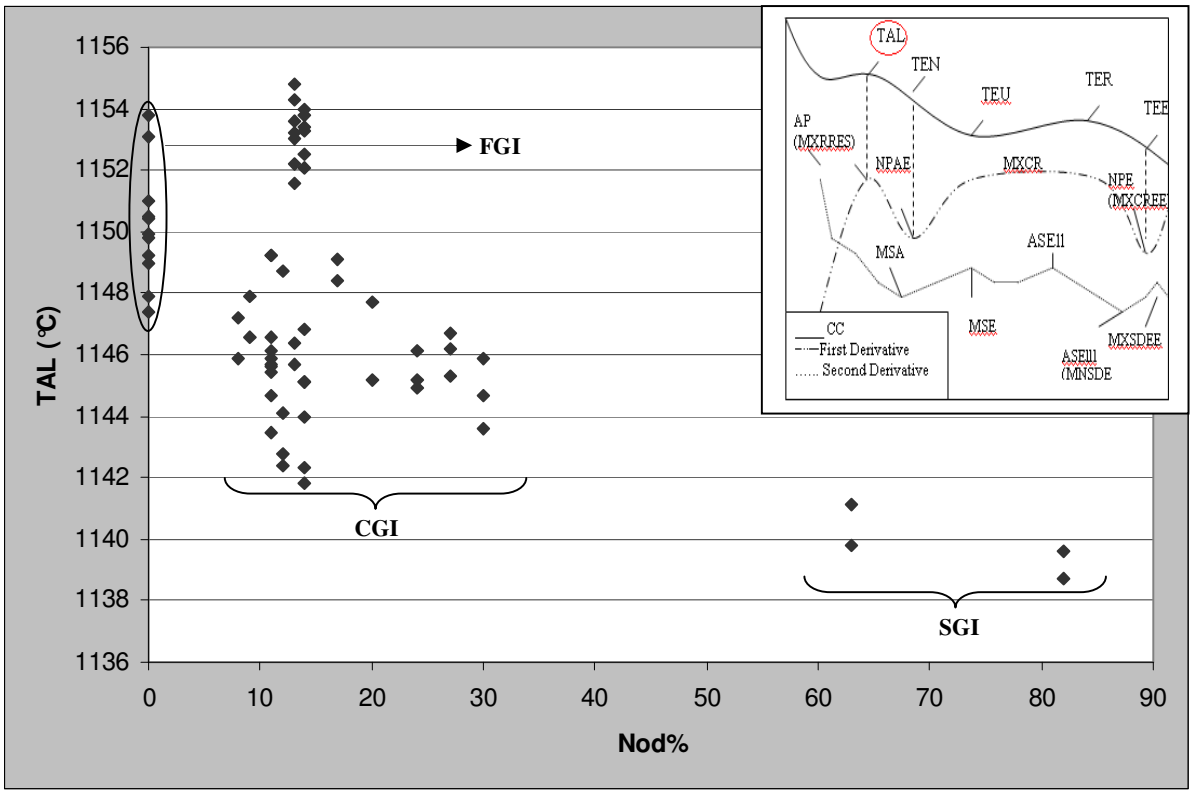

Figure 27. The correlation between the temperature of austenite solidification and nodularity.

4. 5. 2. Temperature of Eutectic Nucleation (TEN or TES)

TEN for CGI in the cast samples falls nearly between SGI and FGI. But there are some overlaps in some temperature points for FGI and CGI which make the distinction difficult. Figure 28 demonstrate the correlation of the TEN and the nodularity value.
This point on the cooling curve is often quite vague and difficult to measure exactly.

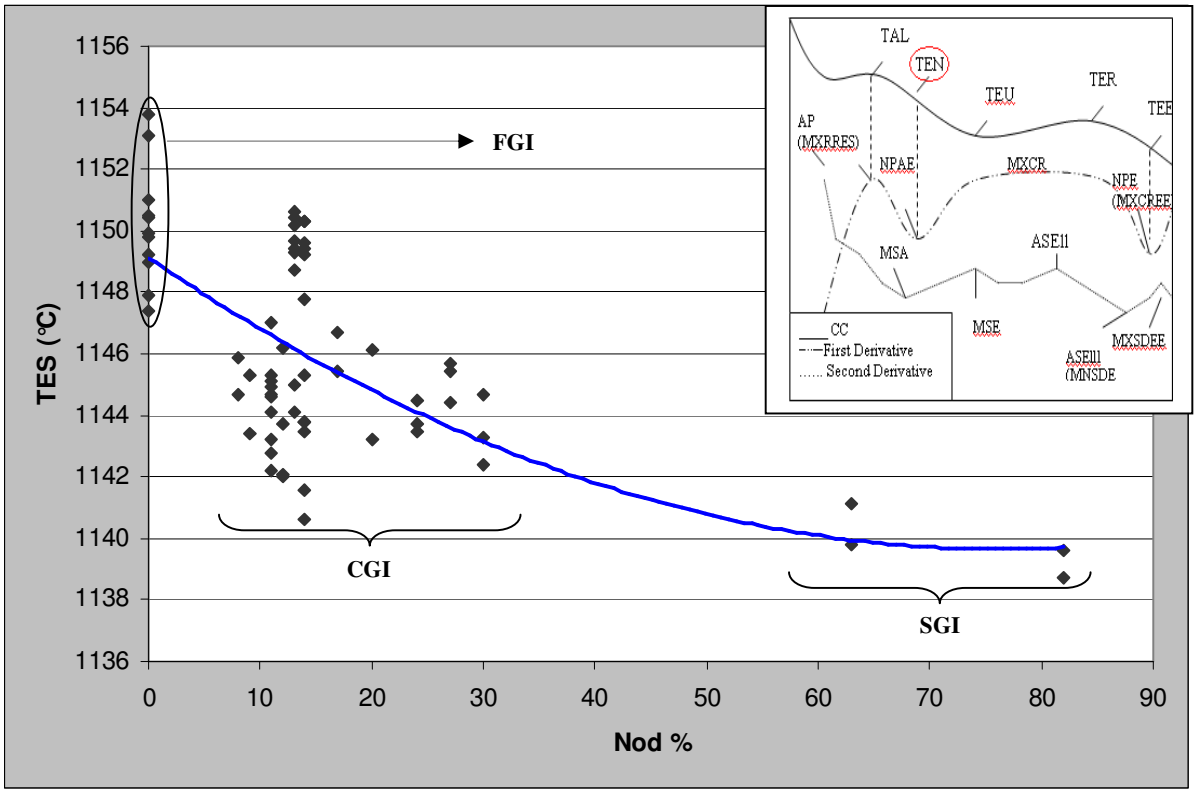

Figure 28. The correlation between the temperature of eutectic nucleation and nodularity.

4. 5. 3. Temperature of Eutectic Undercooling (TEU or TElow)

Stefanescu states that the TEU for CGI has the lowest value in comparison with the other graphite types [4], which is because of unfavourable nucleation condition in CG iron that leads to a delay in solidification. But Bäckerud et al [31] showed that it is possible to have the TEU of CG iron between that of SGI and FGI. As can be seen in figure 29, results achieved from samples are close to the second theory. The interesting point is that there is an obvious difference between the TEU of CG iron and that of FG iron. Even when the CGI sample with the lowest nodularity value is compared with the FGI sample with the lowest TEU, it is evident that the flake one exhibits at least about 2 °C higher temperature than the CGI one. TEU of nearlly all FGI samples are above 1148 °C. Although the TEU of CG iron is higher than that of SG iron, it seems that it is more difficult to distinguish between these two types, since the temperatures are close two each other and in some points even an overlap can be seen.

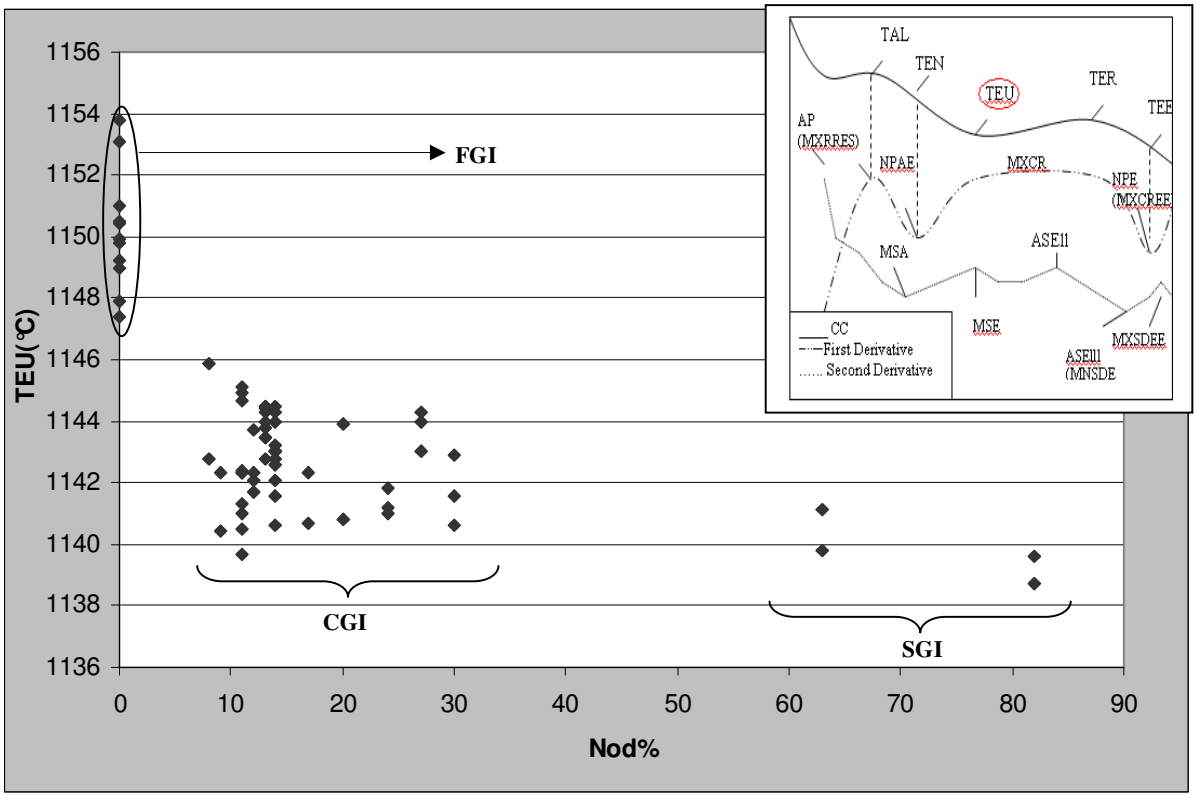

Figure 29. The correlation between the temperature of eutectic undercooling and nodularity

4. 5. 4. Maximum Temperature of Eutectic Arrest (TER or TEhigh)

As mentioned above, because of unfavourable nucleation condition in CG iron, it shows a delay in start of solidification but when it starts to solidify, it proceeds rapidly with a lot of latent heat released which leads to higher TER than SGI [4]. It can be concluded from figure 30 that the trend is like the one in TEU and the points related to CG iron samples lie between those of FGI and SGI. Similar to the temperature of eutectic undercooling, there is a significant difference between the FG and CG irons but coming into the conclusion may become more crucial when comparison is made between two CGI samples with high and low nodularity value. The numerical amount of temperature can be seen in table 6. Again it should be considered that these values are sensitive to different parameters mentioned before and then they can vary by any changes in each of those parameters.

Table 6. TER related to different cast iron samples cast in the project.

Cast Iron Type	Tempereture of Eutectic Arrest (°C)
FG	TER ≥ 1154
CG	1152 ≤ TER ≤ 1146
SG	TER ≤ 1146

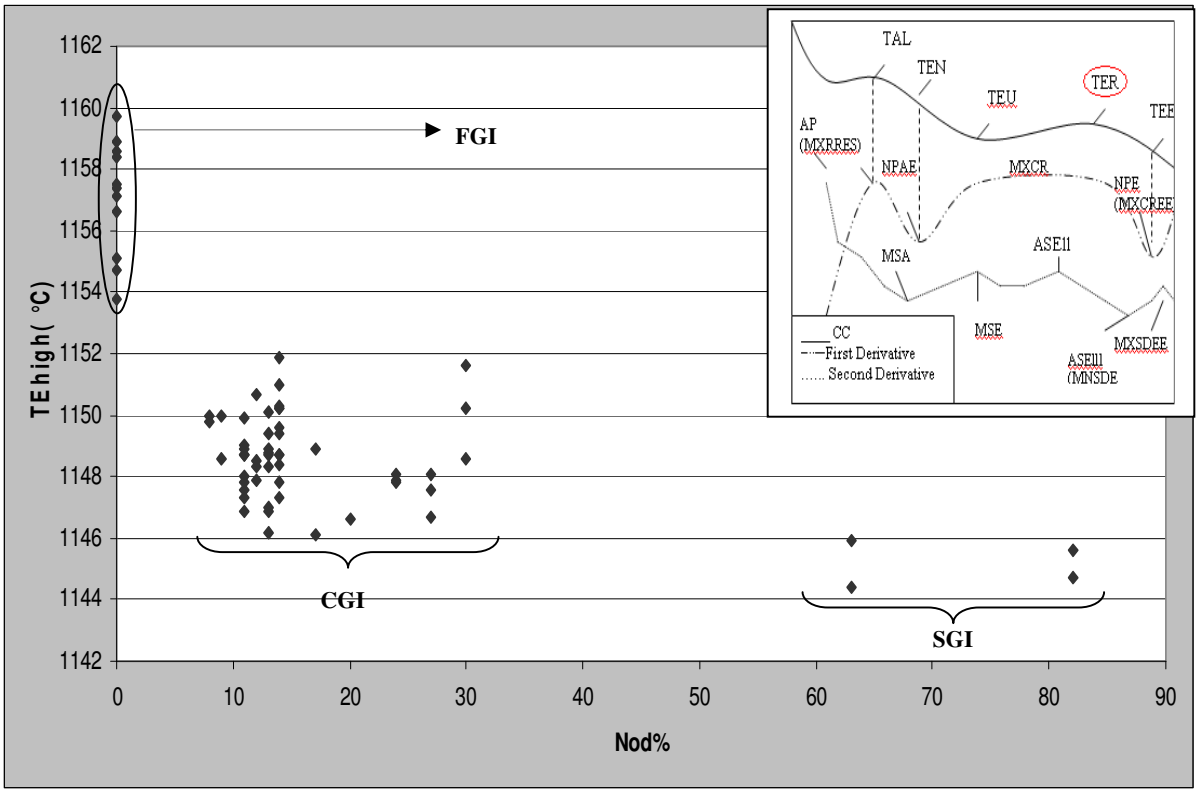

Figure 30. The correlation between temperature of eutectic arrest and nodularity

4. 5. 5. Temperature of Eutectic End (TEE or TS)

It was expected to have TEE for the CGI samples close to that of FG iron and both considerably higher than SGI one. [3] But as it is clear from figure 31, TEE of SGI is even higher than the value of CG. The reason can be described in this way; Addition of magnesium to the melt can cause occurrence of segregation in the microstructure which leads to a lower TEE for CGI in comparison with FGI. But although there is even higher amount of magnesium added in SG iron, it shows higher TEE than CGI. It can be because of existence of smaller unit cells in the SGI than CGI microstructure which causes lower segregation around the cells and eventually leads to the higher TEE.
There is an obvious difference in the TEE of FG and CG irons and the difference in absolute numbers is much larger in comparison with previous characteristic points. But still it is difficult to distinguish between SG and CG irons.

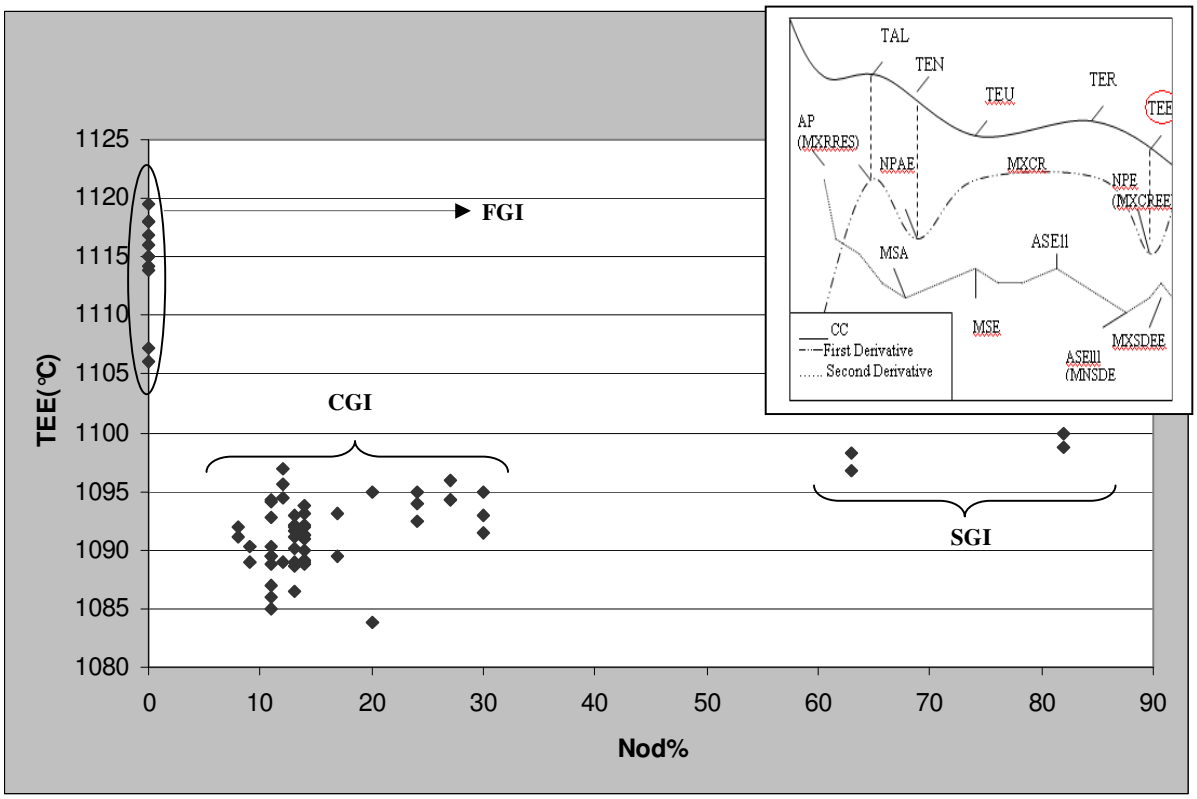

Figure 31. The correlation between the temperature of eutectic end and nodularity.

4. 5. 6. Cooling rate (dT/dt) at TES.

In the samples cast, the cooling rate at the temperature of eutectic nucleation is almost always lower for CG iron than SG and FG irons. But as can be seen there is an overlap in one point (dT/dt = -0.05 °C/Sec) for all three types. Figure 32 demonstrates that nearly all the points related to CGI are located below -0.05 (°C/Sec), while SGI and FGI points are nearly equal and higher than 0.05 (°C/Sec).

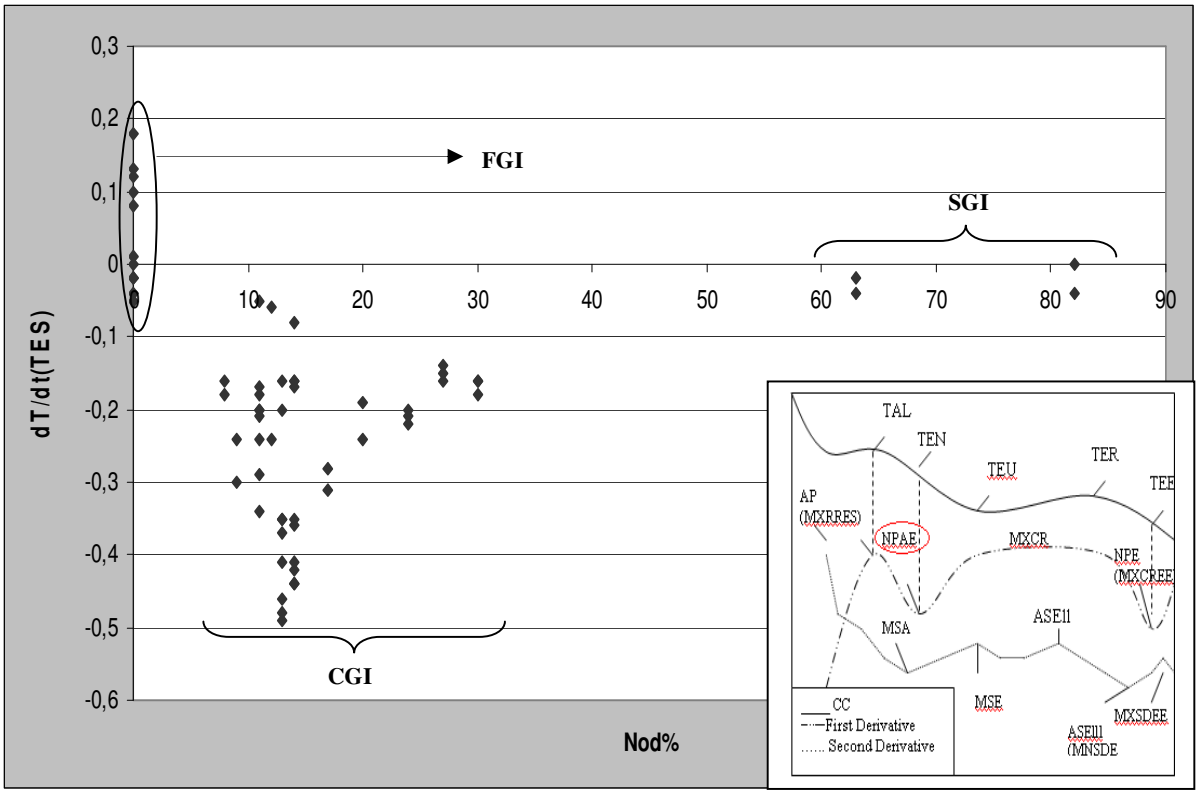

Figure 32. The correlation between the cooling rate at TES and nodularity

4. 5. 7. Maximum Recalescence Rate

It was expected to have considerably higher maximum recalescence rate for CG iron than the other two types [3] but according to the results achieved in the project, no special trend can be defined.

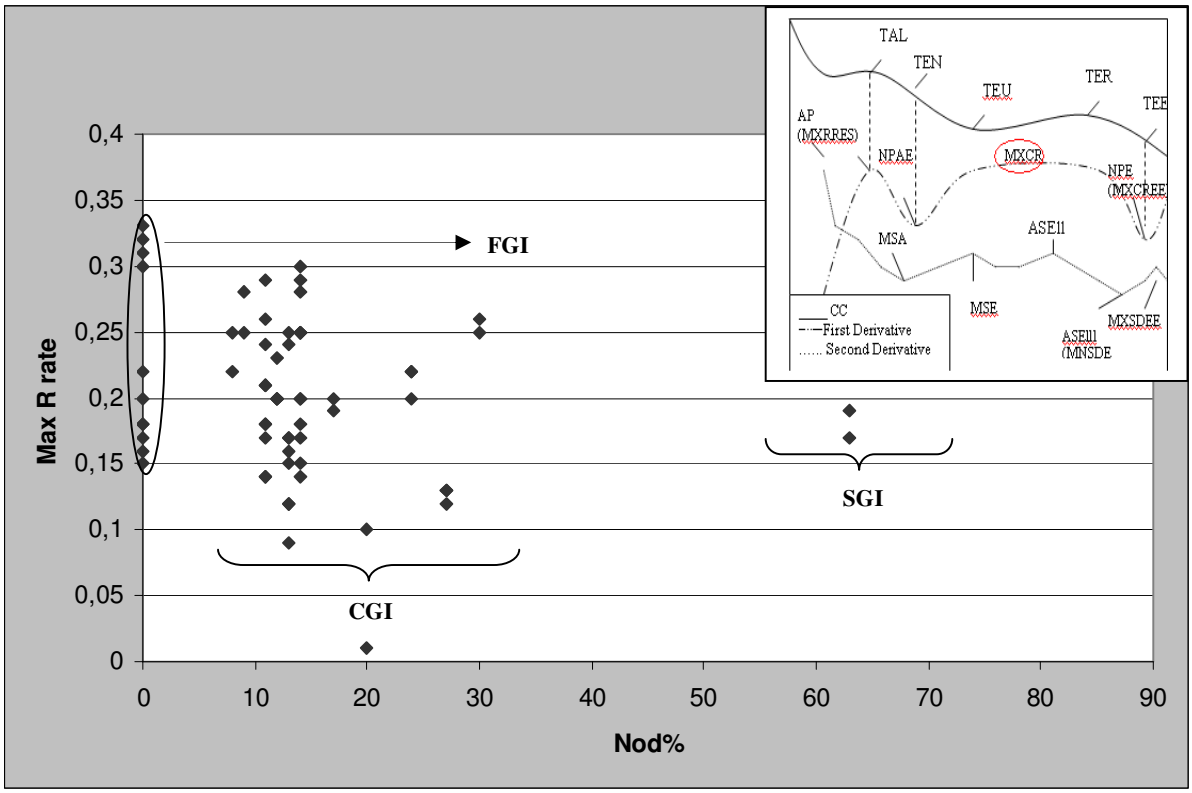

Figure 33. The correlation between max recalescence rate and nodularity

4. 5. 8. Cooling rate (dT/dt) at TEE (TS)

Similar to figure 33, it is not possible to define the type of cast iron by comparing the cooling rate at TEE because the points does not obey any specific trend.

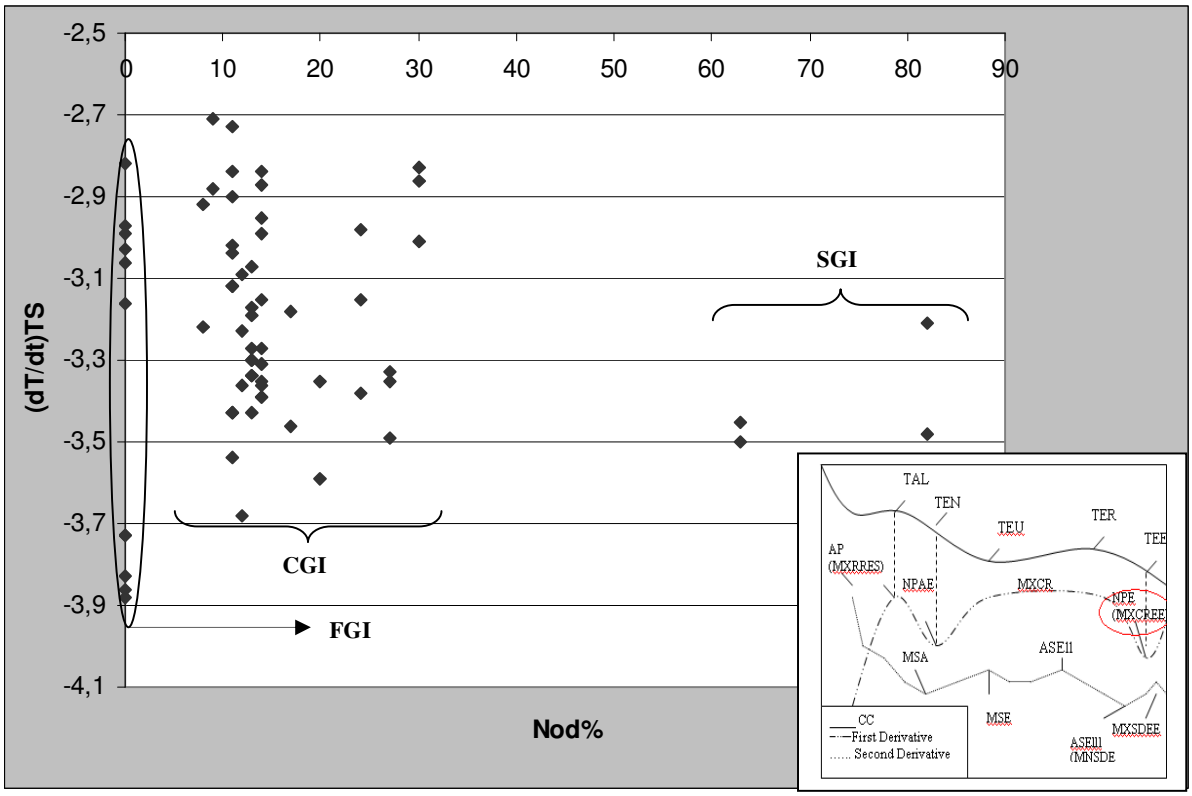

Figure 34. The correlation between the cooling rate at TES and the nodularity value

V. Conclusions

Approach I

The results related to this approach are confidential for the Volvo Company. Any questions can be answered by Pål Schmidt.

Approach II

As demonstrated in figure 26, if the CCs with the same initial temperature are selected, the cooling curves related to the CGI sample lie between the other two types, but it should be considered that there are different parameters (see paragraph 2. 5) which can affect the shape of the cooling curves and their effects can even overlap. Table 6 demonstrates the possibility of recognition of different cast iron types by means of comparing the characteristic points of the cooling curves. Figure 35 shows the correlation between TEU, cooling rate at TES and the nodularity value. It has been seen that in some commercial methods a 3D curve like figure 35 is used to make a combination of correlations between different characteristic points and cast iron types.

Table 7. The possibility of distinguish between different cast iron types by means of comparing the characteristic points.

Characteristic Points	Distinguishability Between Different Cast Iron Types		
	FG and CG	CG and SG	FG and SG
TAL	No	Yes	Yes (easily)
TEN	No	No (overlap)	Yes (easily)
TEU	Yes	No	Yes (easily)
TER	Yes	Yes (overlap)	Yes (easily)
TEE	Yes (easily)	Yes (overlap)	Yes
(dT/dt) at TES	Yes (overlap)	Yes (overlap)	No
Max R rate	No	No	No
(dT/dt) at TEE	No	No	No

It is logical to conclude that;
- The FG and SG irons are easily distinguishable from each other by comparing the TAL, TEN, TEU and TER.
- The FG and CG irons show a considerable difference in TEE. Although the differences are lower at TEU and TER, these two points can also be used to recognise these two types.
- The recognition becomes crucial when the comparison is made between the CG and SG irons. Although these two types exhibit some differences at TAL, TER and TEE, because of the small difference and even existence of some overlaps, it is difficult to state that this approach is applicable for distinction between CG and SG irons. It becomes even more crucial when CG iron with high and low nodularity value are discussed and compared.

Unlike approach II which is not completely applicable for the recognition of different cast iron types, approach I shows distinguishable results which are totally useful to apply in CGI production.

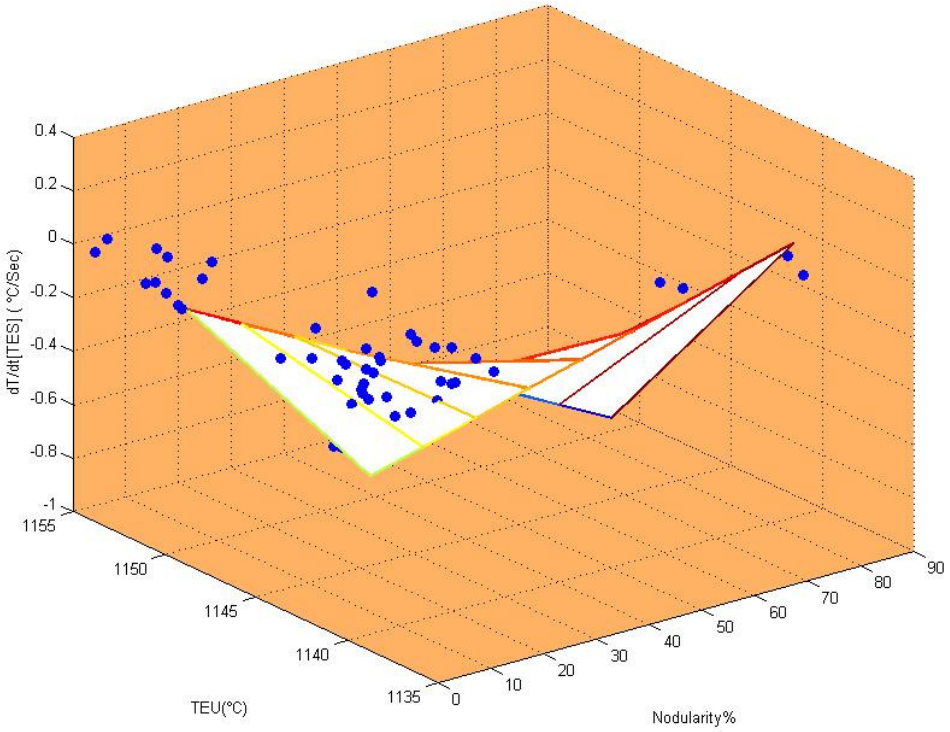

Figure 35. The correlation between TEU, cooling rate at TES, and the nodularity value.

VI . References

[1] G. Cueva, A. Sinatora, W.L. Guesser, A.P. Tschiptschin, Wear 255 (2003)1256–1260.
[2] G.F. Geier,W. Bauer, B.J. McKay, P. Schumacher,Materials Science and Engineering A 413–414 (2005) 339–345.
[3]. D.M.Stefanescu, ‘’Solidification of flake, compacted/vermicular and spheroidal graphite cast irons as revealed by thermal analysis and directional solidification experiments’’ the university of Alabama
[4]. D.M.Stefanescu et al, ‘’Solidification behaviour of hypoeutectic and eutectic Compacted Graphite Cast Irons. Chilling tendency and eutectic cells.’’, AFS transactions
[5]. I. Minkoff, B. Lux, "Graphite Growth from Metallic Solution,"
The Metallurgy of Cast Iron, pp 473-491, Georgi Publishing Co, St.
Saphorin (1975).
[6]. B. Lux, I, Minkoff, F. Mollard, E. Thury, "Brunching of Graphite Crystals Growing from a Metallic Solution," The Metallurgy of Cast Iron, pp 495-508. Georgi Publishing Co, St. Saphorin (1975).
[7] P. Zhu, R. Sha, and Y. Li: The Physical Metallurgy of Cast Iron,Proc. Materials Research Society, H.Fredriksson and M. Hillert,eds., North-Holland, 1985, vol. 34, pp. 3–11.
[8] D.M. Stefanescu, Properties and Selection: Irons, Steels and High PerformanceAlloys, vol. 1, ASM Handbook, 1993, pp. 64–70.
[9] A.N. Roviglione, J.D. Hermida, Metallurgical and Materials Transactions B 236
(33b) (2002 April) 34–40.
[10] C.G. Chao, T.S. Lui, M.H. Hon, Journal of Materials Science 24 (1989) 2610–2614.
[11] ASM Handbooks. Volume 1.principle of the metallurgy of cast iron.
[12] Y.-H. Shy, C.-H. Hsu, S.-C. Lee, C.-Y. Hou, Materials Science and Engineering A278 (2000) 5460.
[13] M.F. de Campos, L.C. Rolim Lopes, P. Magina, F.C. Lee Tavares, C.T. Kunioshi, H.Goldenstein, Materials Science and Engineering A 398 (2005) 164–170.
[14] S.Y. Buni, N. Raman, S. Seshan, S¯adhan¯a 29 (2004 February) 117–127, Part 1.
[15] C.-H. Hsu, S.-C. Lee, Y.-H. Shy,W.-T. Chiou, Materials Science and Engineering A
282 (2000) 115–122.
[16] E.huerta, V.Popovski, Astudy of holding time, fading effects and microstructure in ductile iron. Proceeding of the AFS cast iron inoculation conference
[17] X.J.Sun, Y.X.Li, X.Chen, Controlling melt quality of compacted graphite iron
[18]Sintercast website, http://sintercast.com/data/content/DOCUMENTS/200431721250559afs_paper.pdf
[19] C. Labrecque, M. Gagne, AFS Trans. 106 (1998) 83–90
[20] L. Backerud, K. Nilsson, H. Steen, Proceedings of the International Symposium on the Metall. of Cast Iron, Geneva, Switzerland, 1975, pp. 625–637.
[21] T. Kimura, C.R. Loper Jr., H.H. Cornell, AFS Trans. 88 (1980) 443–450.
[22] D.M. Stefanescu, C.R. Loper Jr., R.C. Voigt, I.G. Chen, AFS Trans. 90(1982) 333–348.
[23] Suarez, 2000; Chen and Stephanescu, 1984; Zhu and Smith
[24] Li Zhenhua, Li Yanxiang, Zhou Rong, Melt Quality Evaluation Of Ductile Iron Pattren Recognition Of Thermal Analysis Cooling Curves
[25] Yanxiang Li,Qiang Wang.Intelligent evaluation of melt iron quality by pattern recognition of thermal analysis cooling curves. Journal of materials processing
[26] X.J.SUN, Y.X.Li, X.Chen., 2008, Identification and evaluation of modification level
For compacted graphite cast iron, p471-480
[27] Chaudhari, M. D., Heine, R. W. and Loper Jr., C. R., AFS Trans,0863, 71, 320
[28] Chen, I, G. And D.M.Stefanescu ,FS Trans.0873,81,836
[29] Fung,C.A. Bartelt,P.F. Bradley, J,and Heine,R,W.Conference Proceedin`s\ Cast Iron IV\ MRS\ 428\ 0889[
[30] C.LABRECQUE_ and M.GAGNE.) Review ductile iron. Fifty years of continuous development (354-358)
[31]. L. Backerud. K. Nilsson, M. Steen, "Study of Nucleation and Growth of Graphite in Magnesium-Treated Cast Iron by Means of Thermal Analysis," *The Metallurgy of Cast Iron,* pp 625-637,Georgi Publishing Co, St Saphorin (1975).

[32] N.C. Ghirsovitch, et al., Cast Iron Handbook (in Russian), Leningrad, Masinostrojenie, p 17 (1978).
[33] Svensson, B., 2006. Commercializing CGI, diesel progress. Int. Ed.
[34] M. D. Chaudhari, R. W. Heine, C. R. Loper, Principle involved in the use of cooming curves in ductile iron process control. AFS Transactions 74-96
[35] ISO 16112 :2006(E)- Compacted (vermicular) Graphite cast Irons- Classification

VII. Appendix 1.

As it can be seen, by increasing the magnesium content of the samples, microstructure changes from flake to compacted to spheroidal graphite.

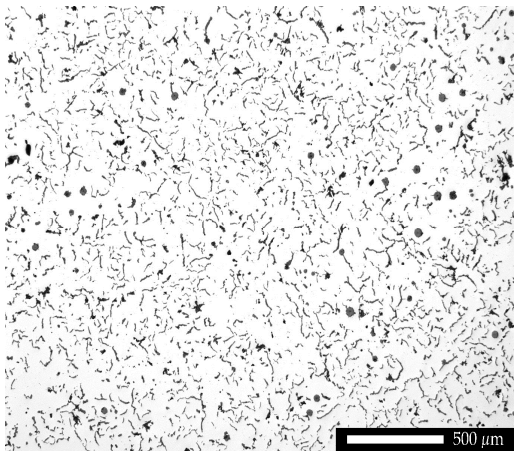

ATAS 1 [0.0094% Mg-14% Nod]

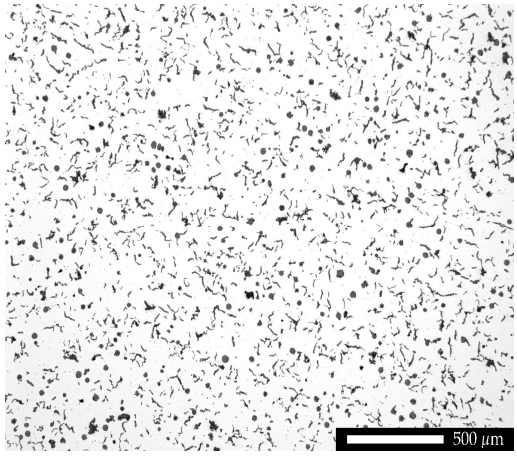

ATAS 4 [0.0099% Mg-17% Nod]

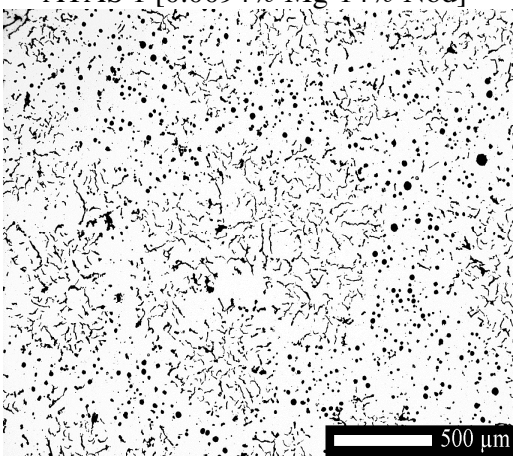

ATAS 21-2 [0.019% Mg-24% Nod]

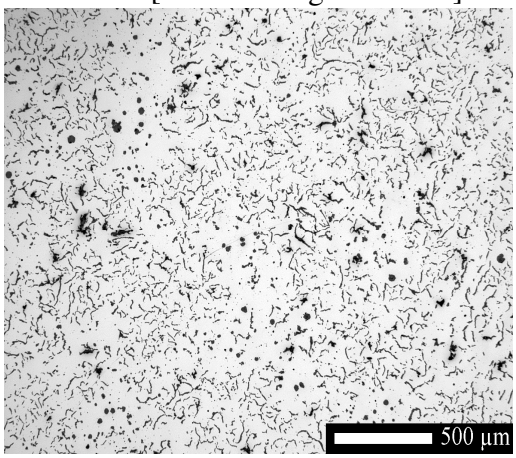

ATAS 15[0.0114% Mg-9% Nod]

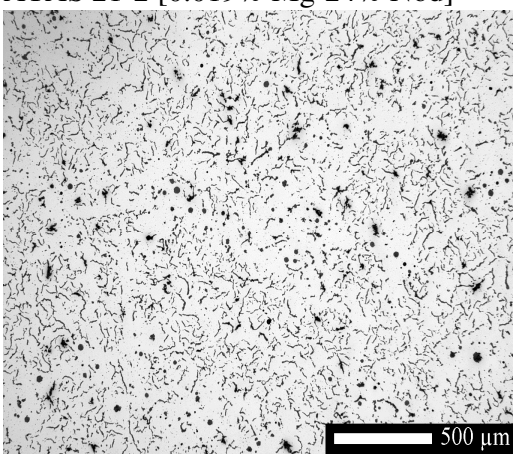

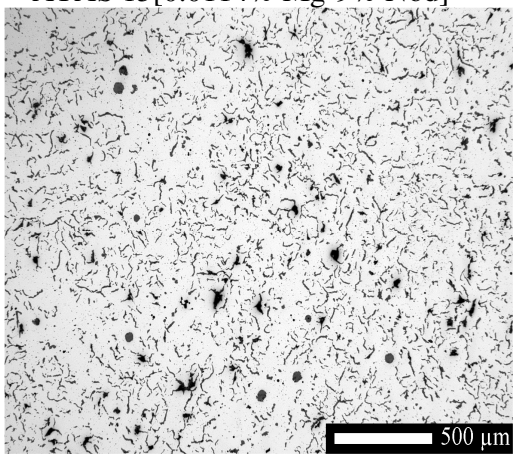

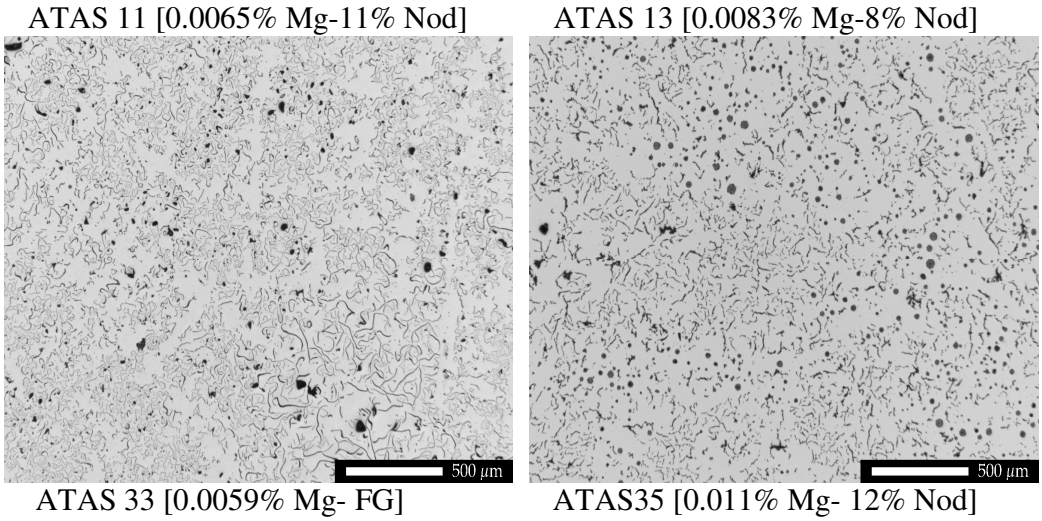

Figure 1 . Graphite morphology in different ATAS samples.

VIII. Appendix 2.

Figure 1. The average of nodularity versus the number of images for sample ATAS 5 based on the Volvo method.

Figure 2. The average of nodularity versus the number of images for sample ATAS 5 based on the ISO standard method.